

*C*ontents

Articles

<i>Special Report on Electrical Standards</i> New Internationally Adopted Reference Standards of Voltage and Resistance	B. N. Taylor	95
A Supercritical Fluid Chromatograph for Physicochemical Studies	Thomas J. Bruno	105
Relation Between Wire Resistance and Fluid Pressure in the Transient Hot-Wire Method	H. M. Roder and R. A. Perkins	113
Scattering Parameters Representing Imperfections in Precision Coaxial Air Lines	Donald R. Holt	117

Conference Reports

Fourth International Symposium on Resonance Ionization Spectroscopy and Its Applications	J. P. Young	135
--	--------------------	-----

Departments

News Briefs

DEVELOPMENTS

137

Conductivity Measurements on Insulating Foams
Development of Standard Weld Procedures
Characterization of Asphaltic Cements
Structure Modulated Chromium Enhances Wear Performance
Discovery of Pervasive Antiphase Boundaries in Liquid Encapsulated
Czochralski-Grown Semi-Insulating Undoped Gallium Arsenide
Intercomparison of Radiometric Standards in the Near Infrared
New Calculations of Inelastic Mean Free Paths for Low-Energy Electrons in Solids
Optical Probes Developed for Electromagnetic Field Measurements
Too Hot to Handle, but Not to Measure
NIST/IBM Neutron Reflection Studies of Polymer Surfaces and Interfaces
Diamond Films Examined
Successful Validation by the Key Management Validation System
New Probe Characterization Technique Promotes More Efficient Use of Geostationary
Orbit Frequency Space by Communications Satellites
Volt, Ohm Standards to Change Internationally in 1990
Test Instrument to Detect Computer Flaws Patented
Better Sheet Metal Products with Less Waste
Making Invention Pay
1989 National Quality Award Applications Issued
Shedding New Light on Ways to Cut Energy Dollars
Test Can Help Ensure Industrial Chemical Purity
New Calibration Services Offered
Papers Available on Optical Fiber Measurements
Characterizing TEM Cells

STANDARD REFERENCE DATA

143

CRYSTDAT: An Online Research and Analytical Tool
Major Expansions Announced for Mass Spectral Database

CALENDAR

144

Special Report on Electrical Standards
***New Internationally Adopted Reference
Standards of Voltage and Resistance***

Volume 94

Number 2

March–April 1989

B. N. Taylor

National Institute of Standards
and Technology,
Gaithersburg, MD 20899

This report provides the background for and summarizes the main results of the 18th meeting of the Consultative Committee on Electricity (CCE) of the International Committee of Weights and Measures (CIPM) held in September 1988. Also included are the most important implications of these results. The principal recommendations originating from the meeting, which were subsequently adopted by the CIPM, establish new international reference standards of voltage and resistance based on the Josephson effect and the quantum Hall effect, respectively. The new standards, which are to come into effect starting January 1, 1990, will result in improved uniformity of electrical measurements worldwide and their consistency with the International System of Units or SI. To implement the CIPM recommendations in the U.S. requires that, on January 1, 1990, the value of the U.S.

representation of the volt be increased by about 9.26 parts per million (ppm) and the value of the U.S. representation of the ohm be increased by about 1.69 ppm. The resulting increases in the U.S. representations of the ampere and watt will be about 7.57 ppm and 16.84 ppm, respectively. The CCE also recommended a particular method, affirmed by the CIPM, of reporting calibration results obtained with the new reference standards that is to be used by all national standards laboratories.

Key words: CCE; CIPM; Consultative Committee on Electricity; International Committee of Weights and Measures; International System of Units; Josephson effect; Josephson frequency-to-voltage quotient; ohm; quantum Hall effect; quantized Hall resistance; SI; volt.

Accepted: December 7, 1988

1. Background

The 18th meeting of the Consultative Committee on Electricity (CCE) of the International Committee of Weights and Measures (CIPM) was held September 27 and 28, 1988, at the International Bureau of Weights and Measures (BIPM), which is located in Sèvres (a suburb of Paris), France. NIST Director E. Ambler, a member of the CIPM and President of the CCE, chaired the meeting and the author attended as NIST representative. Some 30 individuals from 15 countries participated.

As discussed in this journal in the author's 1987 report on the 17th meeting of the CCE held at the BIPM in September 1986 [1], the CCE is one of

eight CIPM Consultative Committees which together cover most of the areas of basic metrology. These Committees give advice to the CIPM on matters referred to them. They may, for example, form "Working Groups" to study special subjects and make specific proposals to the CIPM concerning changes in laboratory reference standards and in the definitions of units. As organizational entities of the Treaty of the Meter, one of the responsibilities of the Consultative Committees is to ensure the propagation and improvement of the International System of Units or SI, the unit system used throughout the world. The SI serves as a basis for

the promotion of long-term, worldwide uniformity of measurements which is of considerable importance to science, commerce, and industry.

However, scientific, commercial, and industrial requirements for the long-term repeatability and worldwide consistency of voltage and resistance measurements often exceed the accuracy with which the SI units for such measurements, the volt¹ and the ohm, can be readily realized. To meet these severe demands, it is necessary to establish representations¹ of the volt and ohm that have a long-term reproducibility and constancy superior to the present direct realizations of the SI units themselves.

Indeed, as discussed by the author in reference [1], in 1972 the CCE suggested that the national standards laboratories adopt 483 594 GHz/V exactly as a conventional value of the Josephson frequency-to-voltage quotient for use in maintaining an accurate and reproducible representation of the volt by means of the Josephson effect. While most national laboratories did adopt this value, three decided to use different values. Moreover, it has become apparent that the CCE's 1972 value of this quotient is about 8 parts per million (ppm) smaller than the SI value, implying that representations of the volt based on the 1972 value are actually about 8 ppm smaller than the volt.

It has also become apparent that because most national standards laboratories base their representation of the ohm on the mean resistance of a particular group of wire-wound resistors, the various national representations of the ohm differ significantly from each other and the ohm, and some are drifting excessively. Although the Thompson-Lampard calculable capacitor can be used to realize the ohm with an uncertainty² of less than 0.1 ppm, it is a difficult experiment to perform routinely. Hence, the 1980 discovery of the quantum

Hall effect (QHE) by K. von Klitzing [6] was enthusiastically welcomed by electrical metrologists because it promised to provide a method for basing a representation of the ohm on invariant fundamental constants in direct analogy with the Josephson effect. The QHE clearly had the potential of eliminating in a relatively straightforward way the problems of nonuniformity of national representations of the ohm, their variation in time, and their inconsistency with the SI.

To address the problems associated with current national representations of the volt and ohm as discussed above, the CCE at its 17th meeting established through Declaration E1 (1986),³ "Concerning the Josephson effect for maintaining the representation of the volt," the CCE Working Group on the Josephson Effect. The CCE charged the Working Group to propose a new value of the Josephson frequency-to-voltage quotient consistent with the SI value based upon all relevant data that became available by June 15, 1988. Similarly, recognizing the rapid advances made in understanding the QHE since its comparatively recent discovery, the CCE established through Declaration E2 (1986),³ "Concerning the quantum Hall effect for maintaining a representation of the ohm," the Working Group on the Quantum Hall Effect. The CCE charged the Working Group to (i) propose to the CCE, based upon all relevant data that became available by June 15, 1988, a value of the quantized Hall resistance consistent with the SI value for use in maintaining an accurate and stable national representation of the ohm by means of the QHE; and (ii) develop detailed guidelines for the proper use of the QHE to realize reliably such a representation.⁴

Further, the CCE stated its intention to hold its 18th meeting in September 1988 with a view to recommending that both the proposed new value of the Josephson frequency-to-voltage quotient and the proposed value of the quantized Hall resistance come into effect on January 1, 1990. These values would be used by all those national standards

¹ The volt is the SI unit of electromotive force (emf) and electric potential difference. Occasionally it may be referred to in the literature as the absolute volt. As-maintained volt, representation of the volt, laboratory representation of the volt, "national unit of voltage", "laboratory unit of voltage", "practical realization of the volt", and other similar terms are commonly used to indicate a "practical unit" for expressing measurement results. However, to avoid possible misunderstanding, it is best not to use the word *unit* in this context. The only unit of emf in the SI is, of course, the volt. In keeping with references [2] and [3], from which this report has drawn heavily, we use the expression *representation of the volt* and variations thereof. The expression *reference standard of voltage* is also used occasionally in a similar or related sense. The situation for the ohm and resistance is strictly analogous.

² Throughout, all uncertainties are meant to correspond to one standard deviation estimates in keeping with CIPM Recommendation 1 (CI-1986) [4,5].

³ The complete declaration is given in reference [1], but see also references [5] and [7].

⁴ The members of the CCE Working Group on the Josephson Effect were R. Kaarls, Van Swinden Laboratorium (VSL), The Netherlands; B. P. Kibble, National Physical Laboratory (NPL), U.K.; B. N. Taylor, (NIST); and T. J. Witt, Coordinator (BIPM). The members of the CCE Working Group on the Quantum Hall Effect were F. Delahaye (BIPM); T. Endo, Electrotechnical Laboratory (ETL), Japan; O. C. Jones (NPL); V. Kose, Physikalisch-Technische Bundesanstalt (PTB), F. R. G.; B. N. Taylor, Coordinator (NIST); and B. M. Wood, National Research Council of Canada (NRCC), Canada.

laboratories (and others) that base their representation of the volt on the Josephson effect, and that choose to base their representation of the ohm on the QHE. These proposals of the CCE were subsequently approved by the CIPM [8] and by the General Conference of Weights and Measures (CGPM) [9] under whose authority the CIPM functions.

In response to the CCE's directives, each Working Group prepared a report which focused on the review and analysis of the values of the Josephson frequency-to-voltage quotient or quantized Hall resistance in SI units that were available by June 15, 1988; and the derivation of a recommended value for the purpose of establishing an accurate and internationally uniform representation of the volt and of the ohm based on the Josephson effect and on the quantum Hall effect, respectively. Submitted to the CCE in August 1988, the reports include useful background information as well as a discussion as to how the new representations might be used in practice to express calibration results. In keeping with the CCE's charge, the QHE Working Group also prepared a companion report entitled "Technical Guidelines for the Reliable Measurement of the Quantized Hall Resistance." Because unbiased quantized Hall resistance determinations are required for an accurate and reproducible representation of the ohm based on the QHE, these guidelines are of exceptional importance.⁵

2. CCE 18th Meeting Discussion and Principal Decisions

As an aid to the reader, this section of the report also includes some tutorial information.

2.1 Josephson Effect

2.1.1 Definition of Josephson Constant When a Josephson junction is irradiated with microwave radiation of frequency f , its current vs voltage curve exhibits steps at highly precise quantized Josephson voltages U_J . The voltage of the n th step $U_J(n)$, n an integer, is related to the frequency of the radiation by

$$U_J(n) = nf/K_J, \quad (1)$$

where K_J is commonly termed the Josephson frequency-to-voltage quotient [11]. The Working Group on the Josephson Effect (WGJE) proposed that this quotient be referred to as the Josephson constant and, since no symbol had yet been adopted for it, that it be denoted by K_J . It follows from eq (1) that the Josephson constant is equal to the frequency-to-voltage quotient of the $n = 1$ step.

The theory of the Josephson effect predicts, and the experimentally observed universality of eq (1) is consistent with the prediction, that K_J is equal to the invariant quotient of fundamental constants $2e/h$, where e is the elementary charge and h is the Planck constant [11]. For the purpose of including data from measurements of fundamental constants in the derivation of their recommended value of K_J , the WGJE assumed that $2e/h = K_J$. However, K_J is not intended to represent the combination of fundamental constants $2e/h$.

2.1.2 Josephson Effect Reference Standard of Voltage The CCE reviewed the report from the WGJE and discussed at some length the draft recommendation E1 (1988), "Representation of the volt by means of the Josephson effect," prepared jointly by the WGJE and the Working Group on the Quantum Hall Effect. The CCE then agreed:

(i) to use the term "Josephson constant" with symbol K_J to denote the Josephson frequency-to-voltage quotient;

(ii) to accept the WGJE's recommended value of K_J , namely, $K_J = (483\,597.9 \pm 0.2)$ GHz/V, where the 0.2 GHz/V assigned one-standard-deviation uncertainty corresponds to a relative uncertainty of 0.4 ppm;

(iii) to use this recommended value to define a conventional value of K_J and to denote it by the symbol K_{J-90} , so that $K_{J-90} \stackrel{\text{def}}{=} 483\,597.9$ GHz/V exactly. (The subscript 90 derives from the fact that this new conventional value of the Josephson constant is to come into effect starting January 1, 1990, a date reaffirmed by the CCE.) The CCE also noted

(iv) that since K_{J-90} exceeds the CCE's 1972 conventional value of the Josephson constant by 3.9 GHz/V or about 8.065 ppm, the new representation of the volt will exceed that based on the 1972 value by about 8.065 ppm; and further agreed

(v) that because the purpose of the new volt representation is to improve the worldwide uniformity of voltage measurements and their consistency with the SI, laboratories which do not base their national representation of the volt on the Joseph-

⁵ The complete reports of the Josephson and Quantum Hall Effect Working Groups including the "Technical Guidelines" (Rapports BIPM 88/77, 88/8, and 88/9) will appear in the proceedings of the CCE's 18th meeting [2]. Additionally, a combined, somewhat condensed version of the two reports may be found in reference [3] and the "Technical Guidelines" in reference [10].

The theory of the QHE predicts, and the experimentally observed universality of eq (2) is consistent with the prediction, that R_K is equal to the invariant quotient of fundamental constants h/e^2 [13]. For the purpose of including data from measurements of fundamental constants in the derivation of their recommended value of R_K , the WGQHE assumed that $h/e^2 = R_K$. However, in analogy with K_J , R_K is not intended to represent the combination of fundamental constants h/e^2 .

2.2.2 Quantum Hall Effect Reference Standard of Resistance The CCE reviewed the report of the WGQHE and discussed the draft recommendation E2 (1988), “Representation of the ohm by means of the quantum Hall effect,” prepared jointly by the two Working Groups. Because of the similarities between the QHE and the Josephson effect, the review and discussion proceeded expeditiously. Indeed, the second half of point (iii) as given here in section 2.1.2 on the Josephson effect and all of points (v), (vi), and (vii) were viewed by the CCE as applying to the quantum Hall effect as well. Also in analogy with the Josephson effect, the CCE agreed:

(i) to use the term “von Klitzing constant” with symbol R_K to denote the Hall voltage to current quotient or resistance of the $i=1$ plateau;

(ii) to accept the WGQHE’s recommended value of R_K , namely, $R_K = (25\,812.807 \pm 0.005) \, \Omega$, where the $0.005 \, \Omega$ assigned one-standard-deviation uncertainty corresponds to a relative uncertainty of 0.2 ppm; and

(iii) to use this recommended value to define a conventional value of R_K and to denote it by the symbol R_{K-90} , so that $R_{K-90} \stackrel{\text{def}}{=} 25\,812.807 \, \Omega$ exactly.

The same procedure was followed for draft recommendation E2 (1988) as for E1 (1988) regarding the Josephson effect. The final CIPM English language version is as follows:

Representation of the Ohm by Means of the Quantum Hall Effect

Recommendation 2 (CI-1988)

The Comité International des Poids et Mesures, acting in accordance with instructions given in Resolution 6 of the 18th Conférence Générale des Poids et Mesures concerning the forthcoming adjustment of the representations of the volt and the ohm,

considering

—that most existing laboratory reference standards of resistance change significantly with time,

—that a laboratory reference standard of resistance based on the quantum Hall effect would be stable and reproducible,

—that a detailed study of the results of the most recent determinations leads to a value of $25\,812.807 \, \Omega$ for the von Klitzing constant, R_K , that is to say, for the quotient of the Hall potential difference divided by current corresponding to the plateau $i=1$ in the quantum Hall effect,

—that the quantum Hall effect, together with this value of R_K , can be used to establish a reference standard of resistance having a one-standard-deviation uncertainty with respect to the ohm estimated to be 2 parts in 10^7 , and a reproducibility which is significantly better,

recommends

—that $25\,812.807 \, \Omega$ exactly be adopted as a conventional value, denoted by R_{K-90} , for the von Klitzing constant, R_K ,

—that this value be used from 1st January 1990, and not before, by all laboratories which base their measurements of resistance on the quantum Hall effect,

—that from this same date all other laboratories adjust the value of their laboratory reference standards to agree with R_{K-90} ,

—that in the use of the quantum Hall effect to establish a laboratory reference standard of resistance, laboratories follow the most recent edition of the “Technical Guidelines for Reliable Measurements of the Quantized Hall Resistance” drawn up by the Comité Consultatif d’Électricité and published by the Bureau International des Poids et Mesures,

and is of the opinion

—that no change in this recommended value of the von Klitzing constant will be necessary in the foreseeable future.

2.3 Practical Implementation of Recommendations

As implied by the discussion of section 1, the results of voltage and resistance measurements expressed in terms of representations of the volt and ohm based on the Josephson and quantum Hall effects, respectively, will have a higher precision than the same measurement results expressed in terms of the volt and ohm themselves. Indeed, this is one of the principal reasons for establishing such

son effect should, on January 1, 1990, adjust the value of their national volt representation so that it is consistent with the new representation. Further, this consistency should be maintained by having a transportable voltage standard periodically calibrated by a laboratory that does base its representation of the volt on the Josephson effect;

(vi) that even if future, more accurate measurements of K_J indicate that the recommended value differs from the SI value by some small amount, the conventional value K_{J-90} should not be altered. Rather, the CCE could simply note the difference between a representation of the volt based on K_{J-90} and the volt; and

(vii) that because an accurate representation of the volt is important to science, commerce, and industry, laboratories should continue their efforts to realize the volt with greater accuracy, either directly or indirectly via measurements of fundamental constants. This could lead to a significant reduction in the uncertainty assigned to the new volt representation.

Having concurred on these points, the CCE edited the draft recommendation E1 (1988) to bring it to final form. The following week it was submitted to the CIPM for approval at its 77th meeting held on October 4–6, 1988, at the BIPM. After some minor editorial changes, the CIPM adopted it as its own recommendation [12]. The following is the English language version (the French language version is the official one and is given in references [2] and [12]):

Representation of the Volt by Means of the Josephson Effect

Recommendation 1 (CI-1988)

The Comité International des Poids et Mesures, acting in accordance with instructions given in Resolution 6 of the 18th Conférence Générale des Poids et Mesures concerning the forthcoming adjustment of the representations of the volt and the ohm,

considering

—that a detailed study of the results of the most recent determinations leads to a value of 483 597.9 GHz/V for the Josephson constant, K_J , that is to say, for the quotient of frequency divided by the potential difference corresponding to the $n = 1$ step in the Josephson effect,

—that the Josephson effect together with this value of K_J can be used to establish a reference standard of electromotive force having a one-standard-deviation uncertainty with respect to the volt

estimated to be 4 parts in 10^7 , and a reproducibility which is significantly better,

recommends

—that 483 597.9 GHz/V exactly be adopted as a conventional value, denoted by K_{J-90} , for the Josephson constant, K_J ,

—that this new value be used from 1st January 1990, and not before, to replace the values currently in use,

—that this new value be used from this same date by all laboratories which base their measurements of electromotive force on the Josephson effect, and

—that from this same date all other laboratories adjust the value of their laboratory reference standards to agree with the new adopted value,

is of the opinion

—that no change in this recommended value of the Josephson constant will be necessary in the foreseeable future, and

draws the attention of laboratories to the fact that the new value is greater by 3.9 GHz/V, or about 8 parts in 10^6 , than the value given in 1972 by the Comité Consultatif d'Électricité in its Declaration E-72.

2.2 Quantum Hall Effect

2.2.1 Definition of the von Klitzing Constant The QHE is characteristic of certain high mobility semiconductor devices of standard Hall-bar geometry when in a large applied magnetic field and cooled to a temperature of about one kelvin. For a fixed current I through a QHE device there are regions in the curve of Hall voltage vs gate voltage, or of Hall voltage vs magnetic field depending upon the device, where the Hall voltage U_H remains constant as the gate voltage or magnetic field is varied. These regions of constant Hall voltage are termed Hall plateaus. Under the proper experimental conditions, the Hall resistance of the i th plateau $R_H(i)$, defined as the quotient of the Hall voltage of the i th plateau to the current I , is given by

$$R_H(i) = U_H(i)/I = R_K/i, \quad (2)$$

where i is an integer [13]. Because $R_H(i)$ is often referred to as the quantized Hall resistance regardless of plateau number, the Working Group on the Quantum Hall Effect (WQHE) proposed that to avoid confusion, the symbol R_K be used as the Hall voltage-to-current quotient or resistance of the $i = 1$ plateau and that it be termed the von Klitzing constant after the discoverer of the QHE. It thus follows from eq (2) that $R_K = R_H(1)$.

representations.⁶ The question arises, however, as to how such measurement results should be reported in practice. The Working Groups recognized that the potential for significant confusion internationally could best be eliminated by having each national standards laboratory adopt the same approach. To this end, in their reports the Working Groups identified and considered the advantages and disadvantages of three different approaches to the reporting problem, two of which are both rigorous and correct [2]. In the first, new “practical units” “ V_{90} ” and “ Ω_{90} ” are defined; in the second, new, so-called “conventional physical quantities” for electromotive force (and electric potential difference) and resistance, “ E_{90} ” and “ R_{90} ,” are defined.

The CCE discussed at length the three approaches identified by the Working Groups and concluded that there was an alternative solution, similar to the Working Groups’ third approach, that is also rigorous but avoids

(i) defining new practical units of emf and resistance that are likely to differ from the volt and ohm by small amounts and which would be parallel to and thus in competition with the volt and ohm. (Defining such units automatically leads to practical electrical units for current, power, capacitance, etc., thereby giving the appearance that a complete new system of electrical units has been established outside of the SI.) The CCE’s alternative solution also avoids

(ii) defining new conventional physical quantities for emf and resistance which are likely to differ from traditional or true emf and resistance by small amounts. (Defining such quantities automatically leads to conventional physical quantities for current, power, capacitance, etc.; and to the peculiar situation of, for example, the same standard cell having both a conventional emf and a true emf.) Further, the alternative solution avoids

(iii) the use of subscripts or other distinguishing symbols of any sort on either unit symbols or quantity symbols. (With the elimination of such subscripts and symbols, for example, those denoting particular laboratories or dates, the national standards laboratories can avoid giving the impression

⁶ As noted by the CCE [2], the Josephson and quantum Hall effects and the values K_{J-90} and R_{K-90} cannot be used to define the volt and ohm. To do so would require a change in the status of the permeability of vacuum μ_0 from an exactly defined constant, thereby abrogating the definition of the ampere. It would also give rise to electrical units which would be incompatible with the definition of the kilogram and units derived from it.

to the users of their calibration services that there is more than one representation of the volt and of the ohm in general use, that there may be significant differences among national realizations of the new volt and ohm representations, and that either the national realizations or the new representations differ significantly from the SI.)

The CCE’s solution, which was affirmed by the CIPM at its 77th meeting [12] and which all national standards laboratories are requested to follow, is indicated in the following variation of the example given by the CCE [2] (the treatment of resistance measurements is strictly analogous):

The emf E of an unknown standard cell calibrated in terms of a representation of the volt based on the Josephson effect and the conventional value of the Josephson constant K_{J-90} , may be rigorously expressed in terms of the (SI) volt V as (to be specific):

$$E = (1.018\ 123\ 45)\ V \pm \epsilon, \quad (3)$$

where ϵ represents the total uncertainty, in volts, and is composed of the following two components: ΔE , the combined uncertainty associated with the calibration itself and with the realization of the Josephson effect volt representation at the particular standards laboratory performing the calibration; and ΔA , the uncertainty with which the ratio K_{J-90}/K_J is known (i.e., it is assumed that $K_{J-90}/K_J = 1 \pm \Delta A$). According to Recommendation 1 (CI-1988), ΔA is 4 parts in 10^7 or 0.4 ppm (assigned one standard deviation).

Since, by international agreement, ΔA is common to all laboratories, the two uncertainties ΔE and ΔA need not be formally combined to obtain the total uncertainty ϵ but may be separately indicated. Hence, the measured emf E may be expressed as

$$E = (1.018\ 123\ 45)\ V \pm \Delta E \quad (4)$$

for all practical purposes of precision electrical metrology and trade, with ΔA appearing separately on the calibration certificate when the precision of the calibration warrants it. If, for example, $\Delta E/E$ is significantly greater than 0.4 ppm, ΔA may be omitted with negligible effect.

An example of the wording that might be used on a NIST Report of Calibration for a standard cell enclosure for the case where ΔA may not be omitted and which is a variation of the wording given in an example developed by the CCE [2], is as follows:

Sample Hypothetical NIST Calibration Report

This standard cell enclosure was received (date) under power at its normal operating temperature.

The values given in the table below are based on the results of daily measurements of the differences between the emfs of the cells in this standard and those of NIST working standards calibrated in terms of the Josephson effect using the new conventional value of the Josephson constant internationally adopted for use starting January 1, 1990 (see Note A). The measurements were made in the period from (date) to (date).

Cell number	emf (volts, V)	Uncertainty (microvolts, μV)
1	1.018 119 85	0.27
2	1.018 133 77	0.27
3	1.018 126 42	0.27
4	1.018 141 53	0.27

(Information relating to the measurements and their uncertainties to be given here.)

Note A

The value of the Josephson constant used in this calibration, namely, $K_{J-90}=483\,597.9\text{ GHz/V}$ exactly, is that adopted by international agreement for implementation starting on January 1, 1990, by all national standards laboratories that base their national representation of the volt (i.e., their national “practical unit” of voltage) on the Josephson effect. Since all such laboratories now use the same conventional value of the Josephson constant while prior to this date several different values were in use, the significant differences which previously existed among the values of some national representations of the volt no longer exist. Moreover, the national standards laboratories of those countries that do not use the Josephson effect for this purpose are requested to maintain their own national representation of the volt so as to be consistent with the above conventional value of the Josephson constant, for example, through periodic comparisons with a laboratory that does use the Josephson effect. An ideal representation of the volt based on the Josephson effect and K_{J-90} is expected to be consistent with the volt as defined in the International System of Units (SI) to within an assigned relative one-standard-deviation uncertainty of 0.4 ppm ($0.41\ \mu\text{V}$ for an emf of 1.018 V). Because this uncertainty is the same for all national standards laboratories, it has not been formally included in the uncertainties given in the table. However, its existence must be taken into account when the utmost consistency between electrical and nonelectrical measurements of the same physical quantity is required.

2.4 Future Work on Electrical Units

The ideas agreed upon by the CCE as given in point (vii) in Sect. 2.1.2 on the Josephson effect, and which apply equally as well to the quantum

Hall effect, led the CCE to adopt the following formal recommendation which was also approved by the CIPM at its 77th meeting [12].

Realization of the Electrical SI Units

Recommendation E3 (1988)

The Comité Consultatif d'Électricité

recognizing

—the importance to science, commerce and industry of accuracy in electrical measurements,

—the fact that this accuracy depends on the accuracy of the reference standards of the electrical units,

—the very close ties that now exist between electrical metrology and fundamental physical constants,

—the possibility of obtaining more accurate reference standards of the electrical units either directly from the realizations of their definitions or indirectly from measurements of fundamental constants, and

—the continuing need to compare among themselves independent realizations of the units and independent measurements of fundamental constants to verify their accuracy,

recommends

—that laboratories continue their work on the electrical units by undertaking direct realizations of these units and measurements of the fundamental constants, and

—that laboratories pursue the improvement of the means for the international comparison of national standards of electromotive force and electrical resistance.

3. Conclusion

The apparatus currently being used by the national standards laboratories is such that the total experimental uncertainty associated with a particular national representation of the volt based on the Josephson effect generally lies in the range 0.01 to 0.2 ppm. As a consequence, with the worldwide adoption starting January 1, 1990, of the new conventional value of the Josephson constant K_{J-90} , all national representations of the volt should be equivalent to within a few tenths of a ppm. Similarly, the total experimental uncertainty associated with the measurement of quantized Hall resistances also generally lies in the range 0.01 to 0.2 ppm. Hence, with the worldwide adoption starting on January 1, 1990, of a new representation of the ohm based on the QHE and the conventional value of the von Klitzing constant R_{K-90} , all national representations of the ohm should also be equivalent

to within a few tenths of a ppm. Moreover, these new national volt and ohm representations should be consistent with the volt and the ohm to better than 0.5 ppm.

In the U.S., the value of the present national representation of the volt maintained by NIST will need to be increased on January 1, 1990, by about 9.26 ppm to bring it into agreement with the new representation of the volt. This is sufficiently large that literally thousands of electrical standards, measuring instruments, and electronic systems throughout the Nation will have to be adjusted or recalibrated in order to conform with the new representation. Most other countries will be required to make a similar change in the value of their present representation of the volt as can be seen from figure 1. On the same date, the value of the U.S. representation of the ohm maintained by NIST will need to be increased by about 1.69 ppm to bring it into agreement with the new representation of the ohm based on the quantum Hall effect. This too is an amount which is of significance to many existing standards, instruments, and systems.

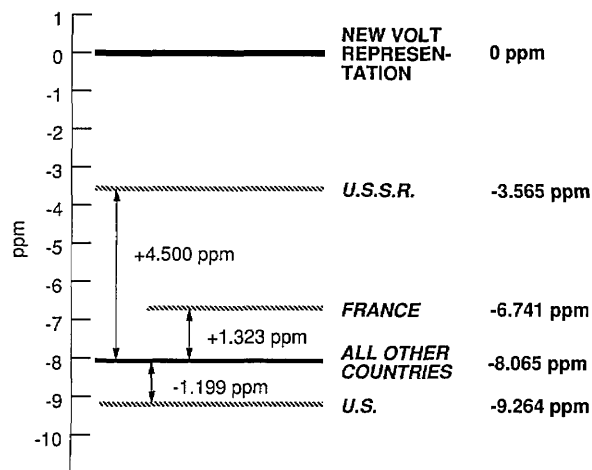


Figure 1. Graphical comparison of the value of the present representation of the volt of various countries as based on the Josephson effect, with the new representation of the volt based on the Josephson effect and the CIPM conventional value of the Josephson constant K_{J-90} which is to come into effect starting on January 1, 1990. The value of the volt representation indicated by "All Other Countries" is based on the conventional value of the Josephson constant stated by the CCE in 1972, namely, 483 594 GHz/V. The countries that currently use this value include Australia, Canada, Finland, F.R.G., G.D.R., Italy, Japan, The Netherlands, and the U.K. The BIPM uses this value as well, but NIST uses 483 593.420 GHz/V. Thus, as the figure shows, on January 1, 1990, the value of the present U.S. volt representation will need to be increased by 9.264 ppm to bring it into conformity with the new representation.

The change required in the value of the national representation of the ohm of other countries varies between a decrease of a few tenths of a ppm to an increase in excess of 3 ppm.

Since $A = V/\Omega$ where A is the ampere as defined in the SI; and $W = V^2/\Omega$ where W is the watt as defined in the SI, the 9.264 ppm and 1.69 ppm increase in the U.S. representation of the volt and of the ohm, respectively, imply that on January 1, 1990, (i) the U.S. representation of the ampere will increase by about 7.57 ppm and (ii) the U.S. electrical representation of the watt will increase by about 16.84 ppm. Because an ideal volt representation based on the Josephson effect and K_{J-90} is expected to be consistent with the volt to within an assigned relative one-standard-deviation uncertainty of 0.4 ppm; and an ideal ohm representation based on the QHE and R_{K-90} is expected to be consistent with the ohm to within an assigned one-standard-deviation uncertainty of 0.2 ppm, ampere and watt representations derived from such ideal volt and ohm representations via the above equations are expected to be consistent with the ampere and watt to within a one-standard-deviation uncertainty of 0.45 ppm and 0.83 ppm, respectively.

The CCE strongly believes, and the author fully concurs, that the significant improvement in the international uniformity of electrical measurements and their consistency with the SI which will result from implementing the new representations of the volt and ohm will be of major benefit to science, commerce, and industry throughout the world; and that the costs associated with implementing the new representations will be far outweighed by these benefits.

About the author: Barry N. Taylor, a physicist, is head of the Fundamental Constants Data Center in the NIST National Measurement Laboratory and Chief Editor of the Journal of Research of the National Institute of Standards and Technology.

4. References

- [1] Taylor, B. N., J. Res. Natl. Bur. Stand. **92**, 55 (1987).
- [2] BIPM Com. Cons. Électricité **18** (1988), to be published.
- [3] Taylor, B. N., and Witt, T. J., Metrologia **26**, No. 1 (1989), to be published.
- [4] BIPM Proc.-Verb. Com. Int. Poids et Mesures **54**, 35 (1986). See also Kaarls, R., BIPM Proc. Verb. Int. Poids et Mesures **49**, A1, 26 (1981); and Giacomo, P., Metrologia **18**, 41 (1982).
- [5] Giacomo, P., Metrologia **24**, 45 (1987).
- [6] v. Klitzing, K., Dorda, G., and Pepper, M., Phys. Rev. Lett. **45**, 494 (1980).
- [7] BIPM Com. Cons. Électricité **17**, E6, E88; E10, E92 (1986).
- [8] Reference [4], p. 10.
- [9] BIPM Comptes Rendus 18^e Conf. Gén. Poids et Mesures, p. 100 (1987). See also Giacomo, P., Metrologia **25**, 113 (1988).
- [10] Delahaye, F., Metrologia **26**, No. 1 (1989), to be published.
- [11] Clarke, J., Am. J. Phys. **38**, 1071 (1970).
- [12] BIPM Proc.-Verb. Com. Int. Poids et Mesures **56** (1988), to be published.
- [13] The Quantum Hall Effect, eds. R. E. Prange and S. M. Girvin, Springer-Verlag, NY (1987). This book provides a comprehensive review of the quantum Hall effect.

A Supercritical Fluid Chromatograph for Physicochemical Studies

Volume 94

Number 2

March–April 1989

Thomas J. Bruno

National Institute of Standards
and Technology,
Boulder, CO 80303

A supercritical fluid chromatograph has been designed and constructed to make physicochemical measurements, while retaining the capability to perform chemical analysis. The physicochemical measurements include diffusion coefficients, capacity ratios, partition coefficients, partial molar volumes, virial coefficients, solubilities, and molecular weight distributions of polymers. In this paper, the apparatus will be described in detail, with particular attention given to its unique features and capabilities. The

instrument has recently been applied to the measurement of diffusion coefficients of toluene in supercritical carbon dioxide at a temperature of 313 K, and pressures from 133 to 304 bar (13.3–30.4 MPa). The data are discussed and compared with previous measurements on similar systems.

Key words: diffusion coefficients; supercritical fluid chromatography.

Accepted: December 11, 1988

1. Introduction

The methods of chromatography have been applied to physicochemical problems such as thermo-physical property determination for nearly 30 years [1,2]. This application of chromatography to non-analytical problems stems from an understanding of the physical and chemical processes which are known to occur during chromatographic separations [3]. As an example, since hydrogen bonding can play a role in chromatographic separation, we may apply chromatography to the study of hydrogen bonding thermodynamics [4].

The development of chromatography during the last 80 years can be divided into distinct historical periods [5], each with its innovations, fads and failures. During the current period, we have seen the emergence of supercritical fluid chromatography (SFC, in which the carrier is a fluid held above its critical point). Some properties of a typical supercritical fluid can be seen in table 1. The density of

Table 1. Comparison of representative fluid properties

	Gas	Liquid	Supercritical fluid
Density, ρ g/mL	10^{-3}	1	0.7
Diffusivity, D cm ² /s	10^{-1}	5×10^{-6}	10^{-3}
Dynamic viscosity, η g/(cm·s)	10^{-4}	10^{-2}	10^{-4}

the supercritical fluid is very similar to that of a liquid phase. This property explains the greatly enhanced solvation power of the supercritical fluid with respect to the gas phase. The viscosity of the supercritical phase closely resembles that of the gas phase, thus allowing for easy mass transfer. The thermal conductivity (though not shown in table 1)

is also relatively large, as one would expect from density and viscosity considerations. The diffusivity (self-diffusion) of the supercritical phase is intermediate between that of a gas and a liquid. This property gives the supercritical fluid the advantage over liquid-liquid extraction. There are many excellent reviews describing the advantages and applications of SFC, and the reader is referred to these for additional details [6,7].

Most of the applications of SFC found in the literature involve analytical or separation problems. The application to physicochemical studies has been relatively slow due to many experimental difficulties. Nonetheless, SFC has been applied to a number of thermophysical problems by several groups. This has included the measurement of capacity ratios, partition coefficients, binary diffusion coefficients, partial molar volumes, virial coefficients, solubilities, and polymer molecular weight distributions. In this work, the physicochemical supercritical fluid chromatograph has been applied to the measurement of binary diffusion coefficients [8-16]. This diffusion coefficient describes the tendency of the solute to diffuse into the carrier (usually referred to as the solvent).

2. Theory

Chromatographic instruments and methodology has been applied to the measurement of binary diffusion coefficients since the early 1960s [17,18]. The theoretical principles of the so-called peak broadening method were formalized by Taylor and Aris [19-23]. Since many authors have treated the theory in full detail, only a brief summary of the main results will be provided here.

A sharply defined spike of solute (δ -function like) introduced into a laminar stream of a carrier flowing in an uncoated tube will be subject to both convective action along the axis of the tube and molecular diffusion in the radial direction. If the tube is assumed to be straight, the mathematical treatment of Taylor and Aris gives a simple expression for the plate height H :

$$H = \frac{2D_{12}}{u} + \frac{r^2u}{24D_{12}}, \quad (1)$$

where D_{12} is the binary diffusion coefficient of the solute into the carrier (solvent), u is the linear velocity of the mobile phase solvent, and r is the internal radius of the uncoated tube. The plate height H is an important and experimentally accessible

quantity in chromatography, since it describes the efficiency of the chromatographic system [24]. This quantity is the width of a peak (as designated by its variance, σ^2 , in length units as opposed to time units) relative to the distance traversed inside the column or tube (i.e., the length of the tube, L):

$$H = \sigma^2/L. \quad (2)$$

In a straight tube, the concentration profile of the solute in the carrier will become Gaussian-like when $H < 0.02$ m [25]. The same result may be obtained from the Golay equation (mathematical description of capillary gas chromatography) when one assumes a zero thickness for the stationary phase film (i.e., an uncoated tube) [26]. At the carrier fluid velocities encountered in practice, eq (1) reduces to:

$$H = \frac{r^2u}{24D_{12}}, \quad (3)$$

which allows calculation of the binary diffusion coefficient.

3. Experimental

The supercritical fluid chromatograph constructed for this work is shown schematically in figure 1. The main components of the instrument are the solvent delivery system, the sample injection system, the column thermostat, and the detection/quantitation system. Safety devices to prevent column temperature and pressure runaway, and inert gas purging of key components provide for explosion-proof operation.

The solvent delivery system is designed to handle fluids which are either gaseous or liquid at room temperature and pressure. The pump is a modified commercial, double piston pressure-controlled device which is electronically compensated for pressure pulsation. This pump is capable of delivering a pressure of 100 MPa, and all associated transfer lines are rated to safely accommodate this limit. The pump head is enshrouded by a welded-seam stainless steel (304) cover (0.16-cm thickness), the inner surface of which is insulated with a 1.27-cm layer of foamed silica. Brazed to the front surface of the cover is a 0.79-cm (inside diameter) compression fitting which accepts the cold stream of a Ranque-Hilsch vortex tube. The vortex tube is used to cool the pump head and carrier stream to facilitate delivery of lower critical point fluids such

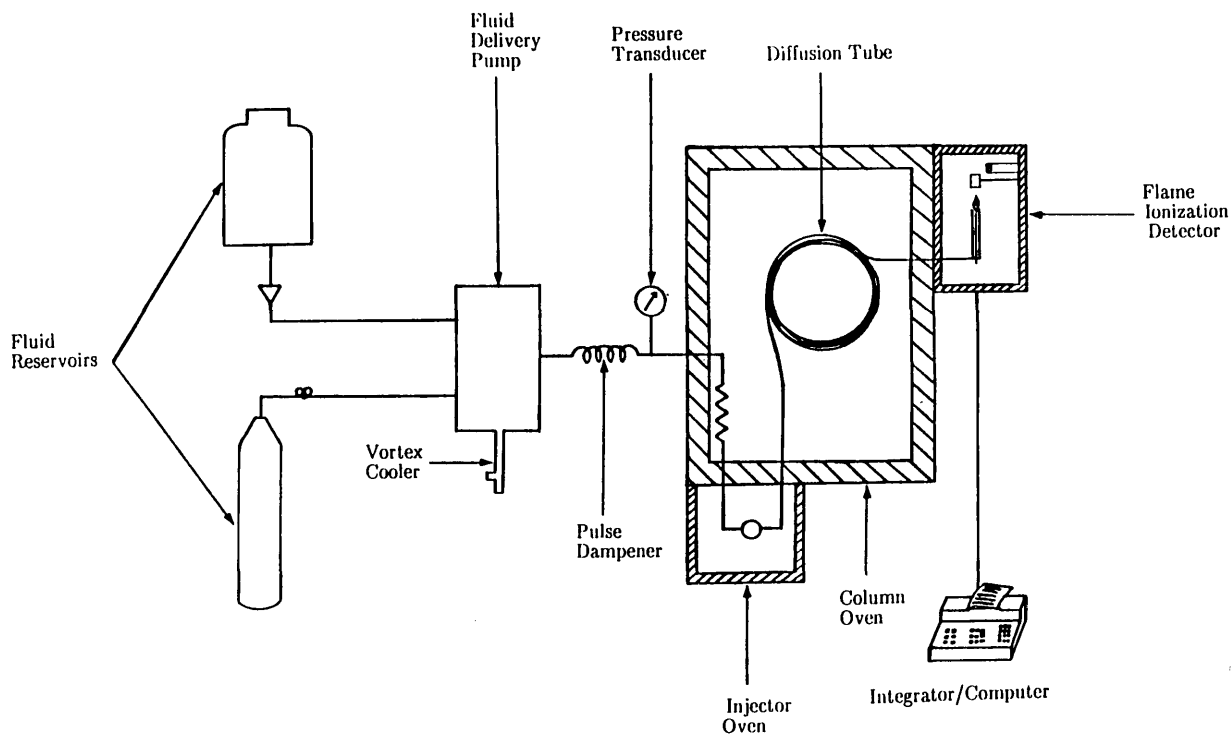


Figure 1. Schematic diagram showing the major components of the supercritical fluid chromatograph used in this work.

as carbon dioxide [27,28]. Before the carrier fluid enters the pump head, it is first passed through a heat exchanger which consists of a 600-cm length of stainless steel (304) tubing (0.076-cm inside diameter, 0.16-cm outside diameter). This heat exchanger insures that fluid is delivered to the pump head as a liquid. The vortex tube is operated in an intermediate mode (between maximum cooling and maximum temperature difference, with an applied air pressure of 0.7 MPa), and provides a carrier stream temperature of -20°C . This minimizes vapor locking and cavitation inside the pump heads.

The pump is followed by a pulse dampener and pressure transducer. The pulse dampener is a coil of flattened stainless steel tubing (0.64-cm outside diameter) which absorbs much of the low level pulsation not handled by the electronic compensation. This component is necessary since no piston pump can operate in true pulse-free fashion. The pressure transducer is a strain gauge device which is calibrated periodically using a high precision Bourdon tube transfer standard. This transfer standard is itself calibrated using a dead weight pressure balance traceable to the NIST primary standard. The uncertainty in the measured pressure has been determined at ± 0.40 bar (± 0.040 MPa).

After leaving the pressure transducer the fluid enters a heat exchanger (fig. 2) inside the column oven, where the flash to supercritical temperature occurs. This heat exchanger is a 300-cm section of stainless steel (304) tubing (0.32-cm outside diameter, 0.07-cm inside diameter). A vibrating tube densimeter is downstream from the heat exchanger, to allow independent density measurements of the carrier if desired. The densimeter places operating constraints upon the entire system (41 MPa maximum pressure, 160°C maximum temperature), and must be removed for higher temperature or pressure operation.

Following the solvent delivery system is the sample injector. The injector used in this work is the flow-through extractor coupled with a high-pressure chromatographic sampling valve shown in figure 3 [29]. This arrangement is most satisfactory for experiments involving repetitive injections of the same solute. An aliquot of solvent-borne sample is syringe-deposited into the extractor. The extractor is then heated and evacuated to remove the sample solvent. After the solvent is removed (an operation which takes approximately 5 minutes), the extractor is filled with the supercritical carrier (solvent) at the same temperature and pres-

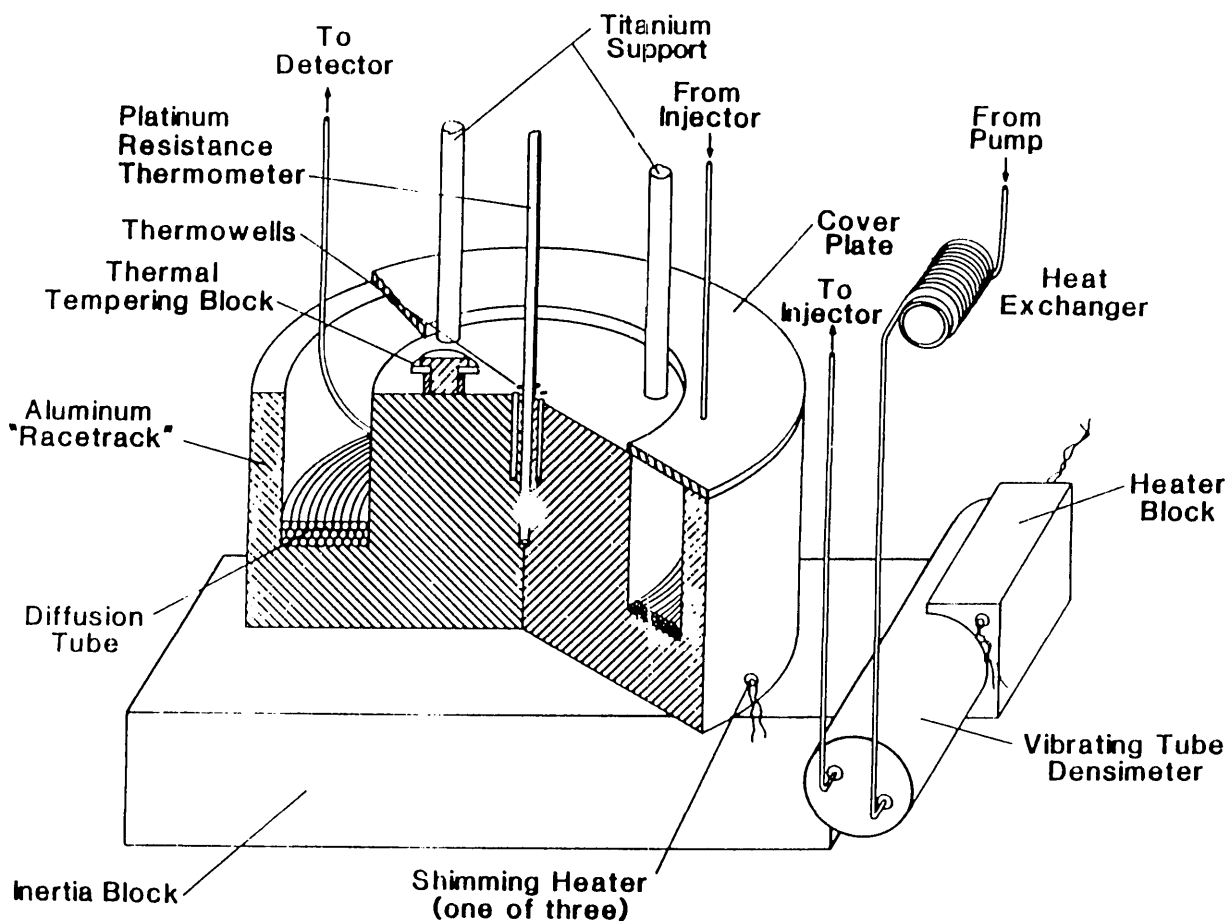


Figure 2. Diagram of the thermostatted column area containing the diffusion tube and vibrating tube densimeter.

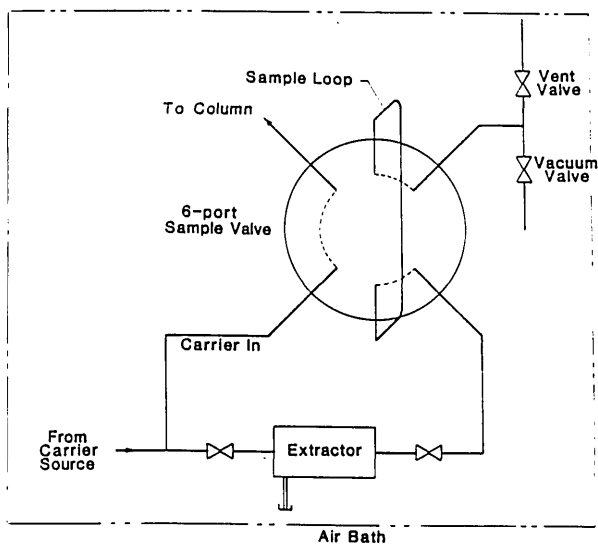


Figure 3. Schematic diagram of the sample injection system.

sure as that in the column. The sample is then loaded into the sample loop to allow injection into the carrier stream. The injection is achieved automatically under computer control using a pneumatic actuator (with helium as the working fluid) equipped with pilot valves and a large ballast volume to provide fast switching.

Upon injection, the carrier-borne solute is transported to the column area (fig. 2) inside of a modified commercial forced-air oven capable of maintaining a temperature of 350 °C. The major modifications to the oven include baffles which promote uniform air movement and an inert gas purge line for safety. The column area contains the heart of the physicochemical experiment, which may consist of a coated or uncoated capillary or a packed column. In the case of diffusion coefficient measurements, the column consists of a long uncoated capillary. This capillary is currently a 3040-cm long continuous section of 316 stainless steel

tubing (0.159-cm outside diameter, 0.025 ± 0.0013 -cm inside diameter) which is connected directly to the injection valve. The length of the diffusion tube was determined by weight, using a calibration equation. This tube is coiled in a 30-cm diameter, held inside of an aluminum racetrack which integrates out local temperature variations. The racetrack also serves as the support for the vibrating tube densimeter referred to earlier. Temperature measurement is provided by a platinum resistance probe located in the center of the racetrack. Six pairs of gradient-sensing thermocouples (type-j, thermally tempered) referenced to the main thermometer provide an indication of temperature nonuniformity. This nonuniformity is then reduced to a negligible level using a set of manually controlled low power shimming heaters. The racetrack is supported inside the oven by titanium rods of 0.64-cm diameter. The low thermal conductivity of the titanium limits heat transfer into or out of the oven. The temperature uniformity of the racetrack has been measured at ± 0.015 °C at temperatures at or above 40 °C.

After leaving the racetrack, the solute is transported to the detector (fig. 4) by the diffusion tube, as shown in figure 2. The detector is a modified chromatographic flame ionization detector contained in a separate oven directly above the column oven. The major modifications made to the commercial unit were in the sample and jet gas inlet lines. Provisions have also been made for the introduction of a make-up gas where needed. A fused

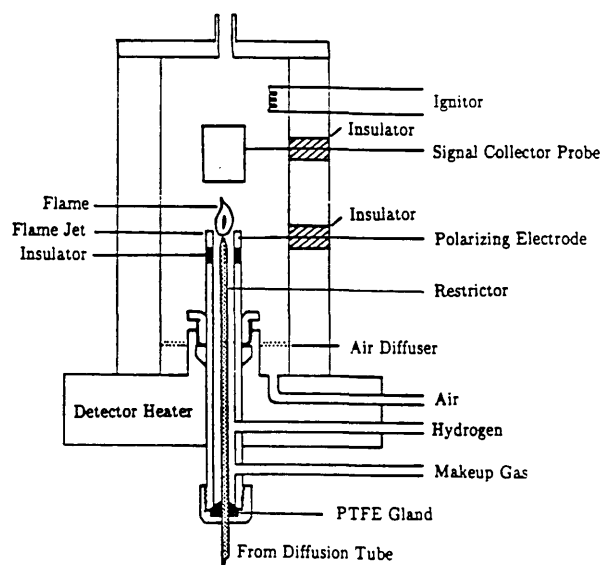


Figure 4. Schematic diagram of the modified flame ionization detector.

quartz capillary restrictor, attached to the diffusion tube, releases the solute and carrier directly into the flame. The detector is operated to provide an approximate sensitivity of 10^{-11} mol/s. The inside diameter and length of this restrictor capillary is chosen so as to maintain the carrier velocity between 2 and 6 cm/s. The temperature of the detector is maintained at 300 °C to prevent the carrier from cooling (and possibly solidifying) upon decompression. This cooling action has been noted as a cause of baseline "spiking" in unheated detectors. The output from the detector is logged on a commercial electronic integrator, from which the retention times and peak widths may be extracted.

4. Results and Discussion

The main sources of error in this experiment stem from the diffusion tube itself, the sample injection process, pressure drop across the tube, and adsorption of the solute on the tube walls. A brief discussion of these errors will be represented here, especially with respect to this apparatus. A number of excellent general reviews are available in the literature [30-34].

The theory of Taylor and Aris, summarized earlier, is strictly based on straight tubes of circular cross-section and uniform inside diameter. For practical reasons the tube is held inside the oven as a helical coil rather than a straight length of tubing. In addition, tubes of perfectly circular cross-section and uniform inside diameter are an idealization not available in the laboratory. We must therefore determine to what extent our experimental apparatus departs from the theoretically assumed conditions. It can be shown [34] that the coiling of the diffusion tube will have no harmful effects if certain criteria are met. The ratio (ω) of the radius of the coil to that of the inside diameter of the diffusion tube should be greater than 100. In the present apparatus, the radius ratio is approximately 1200. Another requirement is that the inequality $De^2Sc < 20$ must be satisfied, where De is the Dean number and Sc is the Schmidt number (see Appendix 1 for definitions). In the design of the present apparatus, De^2Sc is always less than 10. Secondary flow effects are minimized by maintaining the carrier velocity below 6 cm/s, thus assuring flow in the laminar regime.

The problem on nonuniformity of the tubing internal radius is somewhat more difficult to control. It is possible to make corrections for this nonuniformity if the nature of the departure is known

(for example, a sinusoidal variation superimposed on the radius has been considered [34]). Selection of a good quality seamless tubing will help minimize most of the problems associated with tube nonuniformity. It should be noted that the uncertainty in the tube's inside diameter cited in the experimental section (~ 5 percent) is a worst case limit, but this value has been used in the overall error analysis. Since the tube length and radius are both temperature dependent, corrections are applied to account for the effect of thermal expansion on these parameters. The effect of the applied pressure on the internal tube radius is negligible. The effects of connections between the tubes have been minimized by design (only one such connection is used, having the same internal radius as the diffusion tube), and are considered to be negligible.

The errors associated with injection have been addressed in several ways. The sample is introduced at the same pressure and temperature as that of the carrier stream, and at infinite dilution. The volume of the sample loop is very small ($\approx 3.0 \mu\text{L}$) as compared with the volume of the diffusion tube. The sampling loop is switched into the carrier stream only for a short time, and then switched back to the fill position. This has been found to decrease problems from solute adsorption. The injection process is done extremely fast using the pilot valve system, resulting in a negligible pressure pulse.

The pressure drop across the diffusion tube has been measured at between 0.3 and 0.6 bar (0.03–0.06 MPa). Since this is on the order of the experimental error of the pressure measurement, no corrections are made, but close proximity of the critical point is avoided. Measurements made within a few degrees of the critical temperature and near the critical pressure will require consideration of this density gradient effect. Solute adsorption on the inside walls of the tube has not been a problem in the present work, as judged from the peak symmetry. Adsorption is often a problem when using highly polar solutes at relatively low carrier density and temperature. To address this issue, diffusion tubes which have larger internal radii are used so as to decrease the surface area-to-volume ratio. This must be done with consideration of the trade-off in radius ratio ω , and the secondary flow effects which may result.

As an example of the operation of this apparatus, measurements of binary diffusion coefficients of toluene (at infinite dilution) in supercritical carbon dioxide are presented in table 2 [35]. The measurements were made at $313.83 \pm 0.02 \text{ K}$, and at pres-

ures from 133 to 304 bar (13.3 to 30.4 MPa). The carrier fluid density corresponding to these temperature-pressure pairs was calculated from the 32-term Benedict-Webb-Rubin (BRW) equation of state for carbon dioxide [36], and ranged from 0.746 to 0.910 g/cm^3 . As discussed earlier, the raw chromatographic data obtained were the peak widths and breakthrough times (the term "retention time" being considered inappropriate due to the absence of a stationary phase). At each density, 15 separate determinations were made, furnishing the experimental uncertainty for the error analysis. The combined uncertainties of all measured quantities provide an overall estimate of between 5 and 6 percent for the data presented here. The diffusion coefficients are all on the order of $10^{-4} \text{ cm}^2/\text{s}$, and decrease with increasing carrier density as can be seen in figure 5. These data fit in quite well with previous data on lower molecular weight aromatics, although most of the previous data were taken at somewhat lower densities [8–11,14]. Comparisons of this data with several predictive approaches are as yet incomplete and will be presented in the future. Current work also includes a study of a homologous series of straight chain hydrocarbons, and several members of the carotene family.

Table 2. Measured binary diffusion coefficients, D_{12} , of toluene in supercritical carbon dioxide, at $313.83 \pm 0.02 \text{ K}$

CO ₂ density (g/mL)	$D_{12} \times 10^4$ cm ² /s
0.746	1.30
0.801	1.23
0.893	1.21
0.867	1.20
0.890	1.19
0.910	1.19

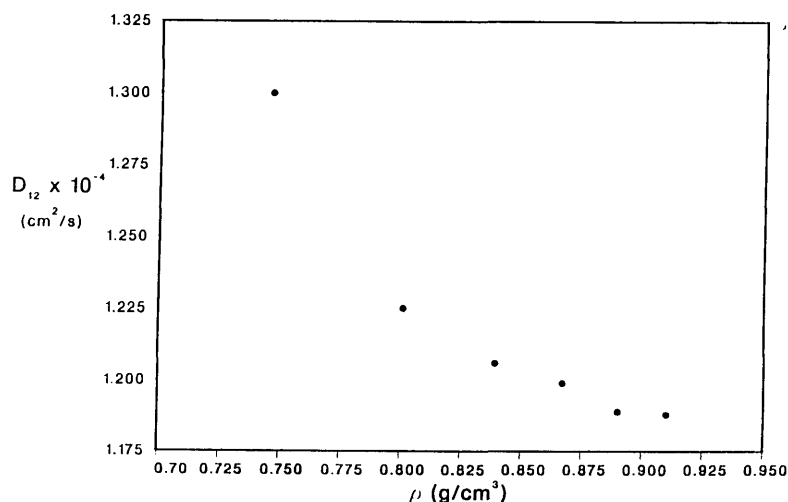


Figure 5. Plot of the binary diffusion coefficient, D_{12} , of toluene in supercritical carbon dioxide at 313.83 K versus the density of supercritical carbon dioxide.

5. Acknowledgment

The financial support of the United States Department of Energy, Office of Basic Energy Sciences, Division of Engineering and Geosciences, is gratefully acknowledged.

About the author: Thomas J. Bruno is a physical chemist in the Thermophysics Division of the National Engineering Laboratory at the National Institute of Standards and Technology, Boulder, CO.

6. References

- [1] Conder, J. R., and Young, C. L., Physicochemical measurement by gas chromatography (John Wiley and Sons, Chichester, 1979).
- [2] Laub, R. J., and Pecsok, R. L., Physicochemical applications of gas chromatography (John Wiley and Sons, New York, 1978).
- [3] Bruno, T. J., Proc. Second Symp. Energy Eng. Sci., Argonne Natl. Lab., CONF-8404123, (1984) pp. 78–85.
- [4] Bruno, T. J., and Martire, D. E., J. Phys. Chem. **87**, 2430 (1983).
- [5] Bruno, T. J., Proc. Fifth Symp. Energy Eng. Sci., Argonne Natl. Lab., CONF-8706187, (1987) pp. 52–60.
- [6] Jackson, W. P., Richter, B. E., Fjeldsted, J. C., Kong, R. C., and Lee, M. L., Ultrahigh resolution chromatography, Ahuja, S., ed., ACS Symposium Series, #250, Washington, D.C. (1984).
- [7] White, C. M., and Houck, R. K., J. High Res. Chromatogr. Chromatogr. Comm. **9**, 3 (1986).
- [8] Van Wassen, V., Swaid, I., and Schneider, G. M., Angew. Chem. Int. Ed. Eng. **19**, 575 (1980).
- [9] Swaid, I., and Schneider, G. M., Ber. Bunsenges. Phys. Chem. **83**, 969 (1979).
- [10] Wilsch, A., Feist, R., and Schneider, G. M., Fluid Phase Equilibria **10**, 299 (1983).
- [11] Laver, H. H., McManigill, D., and Board, R. D., Anal. Chem. **55**, 1370 (1983).
- [12] Feist, R., and Schneider, G. M., Sep. Sci. Tech. **17**, 261 (1982).
- [13] Springston, S. R., and Novotny, M., Anal. Chem. **56**, 1762 (1984).
- [14] Sassiati, P. R., Mourier, P., Claude, M. H., and Rossett, R. H., Anal. Chem. **59**, 1164 (1987).
- [15] Altares, T., J. Polym. Sci., Part C, Polymer Lett. **8**, 761 (1970).
- [16] Hartmann, W., and Klesper, E., J. Polym. Sci. Polymer Lett. **15**, 713 (1977).
- [17] Giddings, J. C., and Seager, S. L., J. Chem. Phys. **33**, 1579 (1960).
- [18] Wasik, S. P., and McCulloh, K. E., J. Res. Natl. Bur. Stand. (U.S.) **73A**, 207 (1969).
- [19] Grushka, E., and Maynard, V., J. Chem. Educ. **49**, 565 (1972).
- [20] Taylor, G., Proc. R. Soc. London **219A**, 186 (1953).
- [21] Taylor, G., Proc. R. Soc. London **223A**, 446 (1954).
- [22] Taylor, G., Proc. R. Soc. London **225A**, 473 (1954).
- [23] Aris, R., Proc. R. Soc. London **235A**, 67 (1956).
- [24] Grob, R. L., Modern Practice of Gas Chromatography, 2nd ed., (John Wiley and Sons, New York, 1985).
- [25] Levenspiel, O., and Smith, K., Chem. Eng. Sci. **6**, 227 (1957).
- [26] Golay, M. J. E., in Gas chromatography, Desty, D. H., ed. (Butterworth, London, 1958).
- [27] Bruno, T. J., J. Chem. Educ. **64**, 987 (1987).
- [28] Bruno, T. J., Liq. Chromatogr. **4**, 134 (1986).

- [29] Bruno, T. J., Solvent-free injection in SFC using sintered glass deposition, *J. Res. Natl. Inst. Stand. Technol. (U.S.)* **93**, 655 (1988).
- [30] Marrero, T. R., and Mason, E., *J. Chem. Phys. Ref. Data* **1**, 3 (1972).
- [31] Balenovic, Z., Myers, M. N., and Giddings, J. C., *J. Chem. Phys.* **52**, 915 (1970).
- [32] Grushka, E., and Kikta, E. J., *J. Phys. Chem.* **78**, 2297 (1974).
- [33] Cloete, C. E., Smuts, T. W., and deClerk, K., *J. Chromatogr.* **121**, 1 (1976).
- [34] Alizadeh, A., Nieto de Castro, C. A., and Wakeham, W. A., *Int. J. Thermophys.* **1**, 243 (1980).
- [35] Bruno, T. J., *Int. J. Thermophys.*, in press.
- [36] Ely, J. F., *Proc. 63rd Gas Processors Assn. Annual Conv.* (1984), p. 9.

Appendix 1

Some important hydrodynamic parameters:

1. Radius ratio:

$$\omega = R_c/a_0$$

where R_c is the overall radius of the coil, and a_0 is the internal radius of the diffusion tube. The effect of diffusion tube coiling may be considered negligible if the radius ratio is greater than 100.

2. Reynolds

number:

$$R_e = 2a_0 \bar{u}_0 \rho / \eta$$

where \bar{u}_0 is the average carrier fluid velocity, ρ is the carrier density, and η is the carrier viscosity. The fluid flow is considered laminar if the Reynolds number is less than 2000.

3. Schmidt

number:

$$Sc = \eta / \rho D_{12}$$

where D_{12} is the binary diffusion coefficient.

4. Dean number:

$$De = Re \omega^{-1/2}$$

The effects of diffusion tube coiling can be considered negligible if $ScDe^2 < 20$.

Relation Between Wire Resistance and Fluid Pressure in the Transient Hot-Wire Method

Volume 94

Number 2

March–April 1989

H. M. Roder and R. A. Perkins

National Institute of Standards
and Technology,
Boulder, CO 80303

The resistance of metals is a function of applied pressure, and this dependence is large enough to be significant in the calibration of transient hot-wire thermal conductivity instruments. We recommend that for the highest possible accuracy, the instrument's hot wires should be calibrated in situ. If this is not possible, we recommend that a value of γ , the relative resistance change with pres-

sure, of $-2 \times 10^{-5} \text{ MPa}^{-1}$ be used to account for the pressure dependence of the platinum wire's resistance.

Key words: fluid; platinum; pressure; resistance; thermal conductivity; transient hot-wire.

Accepted: December 5, 1988

1. Introduction

During the last decade the transient hot-wire has evolved as the primary method for the measurement of thermal conductivity of fluids. In these systems, the wire, usually platinum, is used both as the heating element and as the temperature sensor. The primary variable measured is the change of resistance of the wire as a function of time. The wire is immersed directly in the fluid, and any pressure experienced by the fluid is transmitted to the wire. It is well known that the resistance of metals changes with applied pressure (see, for example, ref. [1]). What is perhaps not widely appreciated is that this effect is substantial enough to be detected at the relatively low fluid pressures encountered in the typical transient hot-wire measurement of thermal conductivity. In this paper we report resistance measurements on 12.5 μm diameter platinum wires as a function of pressure up to 70 MPa.

2. Method

In the transient hot-wire method the resistance-temperature relation of the platinum wires must be defined accurately to achieve reliable results for thermal conductivity measurements. In our versions of this method [2,3] we have opted for a wire calibration in situ. In both the low-temperature version, 70 to 300 K, [2] and the high-temperature version, 300 to 600 K, [3] we use a Wheatstone bridge to measure resistances. Compensation for end effects is provided by placing the long hot wire in one working arm of the bridge and a shorter, compensating, wire in the other. In contrast to most other instruments where times are measured at a null voltage point, in our instruments the voltages developed in the bridge are measured directly as a function of time with a fast digital voltmeter.

Before making each thermal conductivity measurement, the bridge is balanced using a small supply voltage, 50 to 100 mV, to give an output as near to zero as possible. We have one calibrated standard resistor in each side of the bridge. The voltage drops measured across the standard resistors yield the currents in each side of the bridge. Resistances are then determined in terms of voltage drops across the elements of the bridge, that is the hot wires, the leads, and the adjustable balancing resistors. The hot-wire resistances measured during the balancing of the bridge, together with the cell temperatures determined from the calibrated platinum resistance thermometer mounted on the cell, are taken as the in situ calibration of the wires.

As described in reference [2] the resistance relation for each wire was represented by an analytical function of the type,

$$R(T,P) = A + BT + CT^2 + DP, \quad (1)$$

where $R(T,P)$ is the wire resistance, T is the temperature, and P is the applied pressure. The pressure dependence was small, but statistically significant. In the low-temperature system [2] the high-pressure cell closure can accommodate only three leads. These leads are the two current leads and one potential tap at the corner of the bridge. Additional potential taps are placed outside the high-pressure cell. Since there are still short sections of the leads within the cell we cannot measure the voltage drops across each hot wire directly. The leads are steel and copper, and were accounted for by using resistance tables and by measuring the length and diameter of each piece. For the low-temperature system [2] we could not

be certain that the observed pressure dependence resulted only from the platinum wire since other explanations were also possible.

3. Apparatus

During the last three years we have modified and improved the low-temperature system to enable us to measure the thermal diffusivity of the fluid at the same time that we measure the thermal conductivity. The motivation to measure the thermal diffusivity is, of course, to obtain values of the specific heat, C_p . A description of the changes in the system and initial results on argon are given in [4,5]. Most of the changes made to the apparatus improved the measurement of resistance. The theory of the measurement of thermal conductivity by the transient hot-wire method has been given in [6]. For the measurement of thermal diffusivity, the corrections required by the theory had to be evaluated anew [7]. It turned out, not unexpectedly, that accurate measurement of the wire resistance was of the utmost importance.

All of the changes and improvements were also incorporated into our second apparatus, which was designed to operate at higher temperatures [3]. The Wheatstone bridge circuit, shown in figure 1, was changed to improve the accuracy with which the hot-wire resistances and the initial balance condition could be measured. This was accomplished by adding a digital voltmeter to the system capable of measuring voltages to $0.5 \mu\text{V}$ at the 200 mV level. The voltages required in the wire calibration and bridge-balancing cycle are fed to the voltmeter through a new multiplexer. Each arm of the new

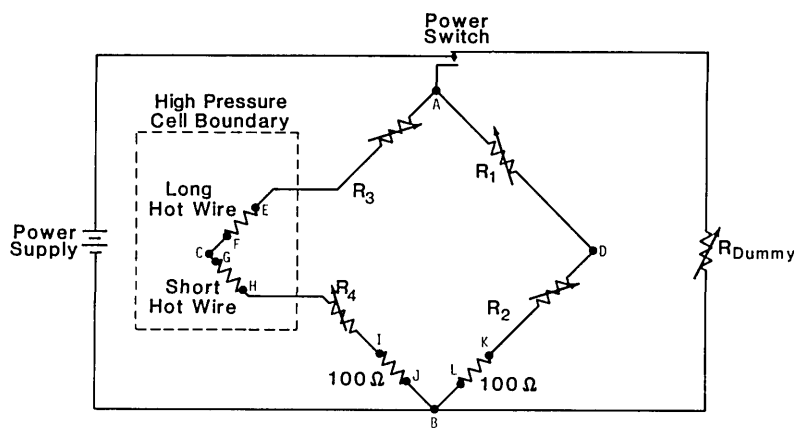


Figure 1. A schematic circuit diagram of the Wheatstone Bridge. Potential taps are indicated by the points A–L.

bridge is about $200\ \Omega$ at ambient temperature and includes a series of precise decade resistances. Because the arms have higher resistances than in the old system, it is possible to include a calibrated $100\ \Omega$ standard resistor in each side of the bridge; thus the current in each side of the bridge can be measured independently.

The new high-temperature apparatus differs in several other aspects from the low-temperature one. Important to the present discussion is the fact that in the new system there are seven leads into the cell rather than three. With the new arrangement of the leads, shown in figure 2, it is now possible to measure the voltages across both the long and the short hot wires directly. This eliminates the need to account for (nuisance) lead resistances and their dependence on temperature within the cell. The resistance measurements are made as follows. With a supply voltage between 50 and 100 mV the current in the left side of the bridge (fig. 1) is determined by measuring the voltage drop across the calibrated $100\ \Omega$ standard resistor at potential taps I and J. The voltage drops across the hot wires are measured between voltage taps E and F, and G and H. The taps are shown in figure 1 while the physical arrangement is shown in figure 2. In summary, we can now measure each resistance with an uncertainty of $9\ \text{m}\Omega$ which is considerably better than the uncertainty of the earliest version of the low-temperature instrument. The measurements described here for nitrogen at 300 K with pressures up to 70 MPa are the first to be made with the new high-temperature system.

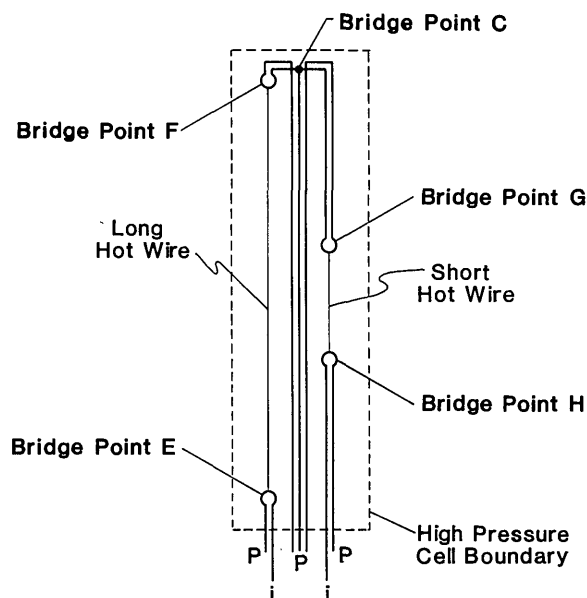


Figure 2. Arrangement of current leads (i) and potential taps (P) within the high pressure cell. Bridge points correspond to those in figure 1.

4. Measurements

Figure 3 shows the measured resistances of both the long and short hot wires as a function of the fluid pressure up to 70 MPa at 300 K. The resistance of each wire clearly decreases as the pressure increases. We represent the data with a straight line for each wire,

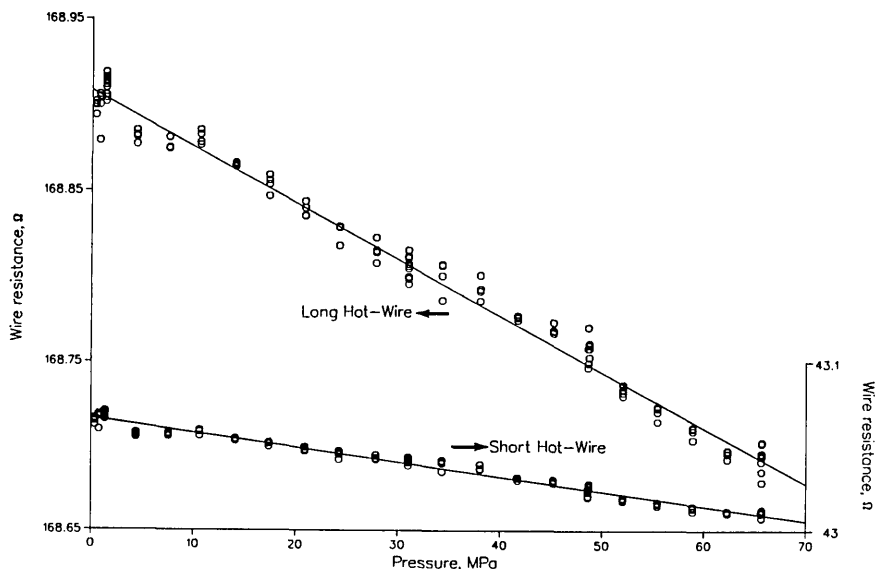


Figure 3. Wire resistance for long and short hot wires as a function of pressure for a temperature of 300 K.

$$R(T,P) = R(T,0) + DP, \text{ or}$$

$$R(T,P)/R(T,0) = 1 + \gamma P. \quad (2)$$

The resistance lines are shown in figure 3; the coefficients and standard deviations are:

	$R(300,0)$ Ω	D $\Omega \text{ MPa}^{-1}$	St. dev. (1σ) Ω	γ MPa^{-1}
long hot wire	168.9085	-0.003 294 46	0.009	-1.95×10^{-5}
short hot wire	43.0667	-0.000 870 63	0.003	-2.02×10^{-5}

In order to compare our results with those of Bridgman [1], we compare the ratios $R(300,70)/R(300,0)$. We obtained a ratio of 0.9986₄ for the long hot wire and 0.9985₉ for the short hot wire. The value interpolated from Bridgman's paper [1] is 0.998₆. The agreement with Bridgman's value is excellent, and we conclude that the measured resistance changes are caused by changes in the fluid pressure. These resistance changes might also be temperature dependent. From the wire calibration established during recent thermal conductivity measurements on nitrogen [8], which were, however, made in the low-temperature system, we obtained values of γ of -1.85×10^{-5} for 250 K and -2.2×10^{-5} for 100 K, a change of about 20 percent in γ .

5. Summary

We close with the recommendation that, if the ultimate in accuracy is to be obtained in a thermal conductivity measurement, an in situ calibration of the hot wires should be performed. If an in situ calibration of the hot wires cannot be performed, then the resistance change of the wires can be taken as an additive, calculated correction using a γ of $-2 \times 10^{-5} \text{ MPa}^{-1}$, as shown in eq (2).

About the authors: H. M. Roder is a physicist and R. A. Perkins is a chemical engineer. Both are involved in the measurement of thermal transport properties of fluids in the Thermophysics Division of the NIST National Measurement Laboratory at Boulder, CO.

6. References

[1] Bridgman, P. W., The resistance of 72 elements, alloys and compounds to 100 000 kg/cm², Proc. Amer. Acad. Arts Sci. **81**, 165 (1952).

[2] Roder, H. M., A transient hot wire thermal conductivity apparatus for fluids, J. Res. Natl. Bur. Stand. (U.S.) **86**, 457 (1981).

[3] Roder, H. M., A high temperature thermal conductivity apparatus for fluids, Proc. of the Fifth Symposium on Energy Engineering Sciences, Instrumentation, Diagnostics, and Material Behavior, June 17–19, Argonne National Lab. Argonne, IL, Dept. of Energy CONF-8706187.

[4] Roder, H. M., and Nieto de Castro, C. A., Heat capacity, C_p , of fluids from transient hot wire measurements, Cryogenics **27**, 312 (1987).

[5] Roder, H. M. and Nieto de Castro, C. A., Measurement of thermal conductivity and thermal diffusivity of fluids over a wide range of densities. Paper presented at the 20th Int. Thermal Cond. Conf.; 1987 Oct 10–21, Blacksburg, Virginia.

[6] Healy, J. J., de Groot, J. J., and Kestin, J., The theory of the transient hot-wire method for measuring thermal conductivity, Physica **82C**, 392 (1976).

[7] Nieto de Castro, C. A., Taxis, B., Roder, H. M., and Wakeham, W. A., Thermal diffusivity measurements by the transient hot-wire technique: a reappraisal, Int. J. Thermophys. **9**, 293 (1988).

[8] Roder, H. M., Perkins, R. A., and Nieto de Castro, C. A., Experimental thermal conductivity, thermal diffusivity and specific heat values of argon and nitrogen, Natl. Inst. Stand. Tech., NISTIR 89-3902; 1988 Oct. 50 p.

Scattering Parameters Representing Imperfections in Precision Coaxial Air Lines

Volume 94

Number 2

March–April 1989

Donald R. HoltNational Institute of Standards
and Technology,
Boulder, CO 80303

Scattering parameter expressions are developed for the principal mode of a coaxial air line. The model allows for skin-effect loss and dimensional variations in the inner and outer conductors. Small deviations from conductor circular cross sections are conformally mapped by the Bergman kernel technique. Numerical results are illustrated for a 7 mm air line. An error analysis reveals that the accuracy of the scattering parameters is limited primarily by

the conductor radii measurement precision.

Key words: Bergman kernel; coaxial air line; conformal mapping; coupling; cubic splines; error sources; measurement contour; measurement precision; principal mode; scattering parameters; skin effect; surface roughness; telegraphist equations.

Accepted: August 1, 1988

1. Introduction

To accurately characterize imperfections of precision coaxial air lines, skin effect and surface roughness need to be considered. Skin effect is now well documented [1] and conductor surface finish has been studied in detail by Rice [2] and Ament [3] through the use of Fourier series methods. While Karbowskiak [4] points out that Fourier analysis reveals useful knowledge of the spectral components which principally affect scattering parameters, it is also appropriate to examine local pointwise influence along the axial (z) coordinate. In this connection, Hill [5] developed perturbation expressions for the scattering parameters for a lossless circular air line. When the conductor surface exhibits transverse angular variation, Rouneliotes, Houssain and Fikioris report the effects of ellipticity and eccentricity on cutoff wave numbers [6].

The purpose of this paper is to develop numerically accurate pointwise coaxial air-line scattering parameters that account for skin effect loss and conductor surface variations in the transverse an-

gular and axial directions. Following Schelkunoff [7], Reiter [8], Solymar [9] and Gallawa [10], generalized telegraphist equations for the principal mode are derived in section 2 for a circular air line. Transformation to forward and backward wave differential equations enables general solutions for the scattering parameters in section 3. To allow for conductor surface measurements along the z -axis, cubic spline polynomials provide a starting point for establishing pointwise recursion formulas of forward and backward waves in section 4. In section 5, the Bergman's kernel technique is used to establish a conformal mapping for transforming noncircular conductors into equivalent circular conductors in correspondence to the principal mode. Computational results illustrating $|S_{11}|$ versus air-line length are given in section 6. An error analysis of the computational algorithms for the accuracy resolution of the measurement system is developed in section 7.

2. Generalized Telegraphist Equations for the Principal Mode

Consider the coaxial air line in figure 1. With inner radius $a(z)$ and outer radius $b(z)$ the field components of primary interest are radial electric field (E_r), angular magnetic field (H_θ), and axial electric field (E_z). We assume the fields E_r , H_θ , and E_z are composed of TEM and TM modes, and coupling of the modes is caused by skin effect with variations of the conductor surfaces. From Appendix A boundary conditions for TM modes possess the form

$$E_z = -Z_s K\{\phi_b(z)\} H_\theta \quad \text{at } r = b(z), \quad (1.0)$$

$$E_z = +Z_s K\{\phi_a(z)\} H_\theta \quad \text{at } r = a(z), \quad (1.1)$$

where for instance,

$$K\{\phi_b(z)\} = \frac{1 + \sin[\phi_b(z)]}{1 + \tan[\phi_b(z)]}. \quad (1.2)$$

Appropriate Maxwell equations for determining transverse fields E_r and H_θ in the air dielectric region of the air line are [11]

$$\frac{\partial E_r}{\partial z} = -j\omega\mu H_\theta + \frac{\partial E_z}{\partial r} \quad (1.3)$$

$$\frac{\partial H_\theta}{\partial z} = -j\omega\epsilon E_r. \quad (1.4)$$

The parameters ω , μ , and ϵ are defined as radian frequency, permeability and permittivity, respectively. In addition the fields are assumed to vary with time according to the complex exponential function $e^{j\omega t}$.

To find the generalized telegraphist equations it is convenient to assume the fields possess orthogonal expansions in r and θ . In view of TEM and TM modes together with impedance boundary condi-

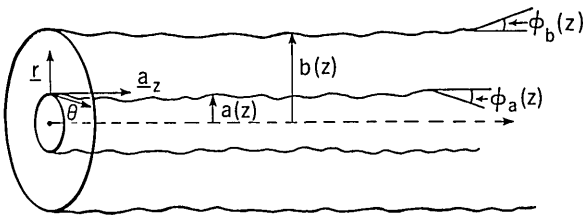


Figure 1. Coaxial air line.

tions a set of orthogonal basis functions needs to be constructed from the Gram-Schmidt process. Assuming E_r , H_θ , and E_z possess continuous first and second derivatives implies their expansions are absolutely and uniformly convergent [12]. In Appendix B these properties are used to rearrange the expansions into the form

$$E_r(r, \theta, z) = \sum_{(n,p)=(0,0)}^{(\infty, \infty)} V_{np}^{(1)}(z) e_{rnp}^{(1)}(r, \theta, z) + V_{np}^{(2)}(z) e_{rnp}^{(2)}(r, \theta, z) \quad (1.5)$$

$$H_\theta(r, \theta, z) = \sum_{(n,p)=(0,0)}^{(\infty, \infty)} I_{np}^{(1)}(z) h_{\theta np}^{(1)}(r, \theta, z) + I_{np}^{(2)}(z) h_{\theta np}^{(2)}(r, \theta, z) \quad (1.6)$$

where the superscripts (1) and (2) represent even and odd modes, respectively. We have

$$\begin{cases} e_{rnp}^{(1)}(r, \theta, z) \\ e_{rnp}^{(2)}(r, \theta, z) \end{cases} = \frac{1}{N_{np}^{-1}(z)} f_{rnp}(r, z) \begin{cases} \cos k\theta \\ \sin k\theta \end{cases}. \quad (1.7)$$

In addition,

$$\mathbf{a}_\theta h_{\theta np}^{(i)}(r, \theta, z) = \mathbf{a}_z \times \mathbf{a}_r e_{rnp}^{(i)}(r, \theta, z); \quad i = 1, 2 \quad (1.8)$$

and $N_{np}(z)$ denotes the norm of $f_{rnp}(r, z)$, that is,

$$N_{np}(z) = \int_{a(z)}^{b(z)} \{f_{rnp}(r, z) \tilde{f}_{rnp}(r, z)\}^{1/2} dr, \quad (1.9)$$

where $\tilde{}$ stands for the complex conjugate. In particular for the TEM mode

$$e_{r00}^{(1)}(r, z) = \frac{1}{N_{00}(z)} \frac{1}{r}, \quad (1.10)$$

$$N_{00}(z) = \left\{ 2\pi \ln \frac{b(z)}{a(z)} \right\}^{1/2}.$$

Higher order modes are usual linear combinations of the first derivative Bessel functions J'_n and Y'_n .

Following Reiter [8] by taking the inner product of eq (1.3) with the basis function $\tilde{e}_{rkq}^{(1)}$ yields

$$\begin{aligned} \int_{S(z)} \frac{\partial E_r}{\partial z} \tilde{e}_{rkq}^{(1)} dS &= -j\omega\mu \int_{S(z)} \mathbf{a}_r H_\theta \cdot \{\mathbf{a}_\theta \tilde{t}_{\theta kq}^{(1)} \times \mathbf{a}_z\} dS \\ &+ \int_{S(z)} \frac{\partial E_z}{\partial r} \tilde{e}_{rkq}^{(1)} dS \end{aligned} \quad (1.11)$$

where $S(z)$ denotes the cross sectional air dielectric region between the conductors. The left side

calls for differentiation of a variable surface integral and the second member of the right side integrates by parts.¹ Hence, eq (1.11) evolves into the form

$$\begin{aligned} & \frac{d}{dz} \int_{S(z)} E_r \tilde{e}_{rkq}^{(1)} dS - \int_{S(z)} E_r \frac{\partial}{\partial z} \tilde{e}_{rkq}^{(1)} dS \\ &= \phi_L \tan\{\theta_b(z)\} E_r \tilde{e}_{rkq}^{(1)} ds \\ & - \phi_L \tan\{\phi_a(z)\} E_r \tilde{e}_{rkq}^{(1)} ds - j\omega\mu \int_{S(z)} H_\theta \tilde{h}_{\theta kq}^{(1)} dS \\ & + \phi_L \{E_z[b(z), \theta, z] - E_z[a(z), \theta, z]\} \tilde{e}_{rkq}^{(1)} ds \\ & - \int_{S(z)} E_z \frac{\partial}{\partial r} \tilde{e}_{rkq}^{(1)} dS. \end{aligned} \quad (1.12)$$

To express E_z in terms of the constructed basis function (f_{np}), let the component of E_z corresponding to $k=0$ (TM_{0p} modes) be expressed as

$$\hat{E}_{z0} = \pi \sum_{p=1}^{\infty} b_{0p}(z) \int_r f_{0p}(u) du. \quad (1.13)$$

From Maxwell's equations the (0p) mode relation between E_r and E_z is

$$\hat{E}_{r,0p}(r, z) = -\frac{\gamma_{0p}}{k_{c,0p}^2} \frac{\partial \hat{E}_{z,0p}}{\partial r} \quad (1.14)$$

where γ_{0p} and $k_{c,0p}$ are the propagation constant and cutoff frequency numbers, respectively. Using eqs (1.5), (1.13), and (1.14) yields

$$b_{0p}(z) = \frac{k_{c,0p}^2}{\gamma_{0p}} N_{np}^{-1}(z) V_{0p}^{(1)}(z). \quad (1.15)$$

Now substituting basis function definitions eq (1.7) and calling for the principal mode yields

$$\begin{aligned} & \frac{dV_{00}}{dz} - 2\pi \sum_{p=0}^{\infty} \int_{a(z)}^{b(z)} \frac{f_{0p}(r, z)}{N_{0p}(z)} V_{0p}^{(1)}(z) \frac{\partial \tilde{f}_{00}(r, z)}{\partial z} \tilde{N}_{00}(z) r dr \\ &= -j\omega\mu I_{00}^{(1)}(z) - 2\pi Z_s K[\phi_b(z)] \frac{\tilde{f}_{00}[b(z), z]}{\tilde{N}_{0p}(z)} b(z). \\ & \sum_{p=0}^{\infty} I_{0p}^{(1)}(z) \frac{f_{0p}[b(z), z]}{N_{0p}(z)} \\ & - 2\pi Z_s K[\phi_a(z)] \frac{\tilde{f}_{00}[a(z), z]}{\tilde{N}_{00}(z)} a(z). \end{aligned}$$

¹ Since $S(z)$ is differentiable and the field components are continuous, interchange of differentiation and integration is justified.

$$\begin{aligned} & \sum_{p=0}^{\infty} I_{0p}^{(1)}(z) \frac{f_{0p}[a(z), z]}{N_{0p}(z)} - \frac{2\pi}{\tilde{N}_{00}(z)} \sum_{p=1}^{\infty} \frac{k_{c,0p}^2}{\gamma_{0p}} \frac{V_{0p}^{(1)}(z)}{N_{0p}(z)} \\ & \int_{a(z)}^{b(z)} \int_r f_{0p}(u) du \frac{\partial}{\partial r} \tilde{f}_{00}(r, z) r dr \\ & + 2\pi \tan[\phi_b(z)] \frac{\tilde{f}_{00}[b(z), z]}{\tilde{N}_{00}(z)} b(z) \sum_{p=0}^{\infty} \frac{f_{0p}[b(z), z]}{N_{0p}(z)} V_{0p}^{(1)}(z) \\ & - 2\pi \tan[\phi_a(z)] \frac{\tilde{f}_{00}[a(z), z]}{\tilde{N}_{00}(z)} a(z) \sum_{p=0}^{\infty} \frac{f_{0p}[a(z), z]}{N_{0p}(z)} V_{0p}^{(1)}(z). \end{aligned} \quad (1.16)$$

To derive the companion generalized telegraphist equation from eq (1.4), the procedure is almost identical. Taking the inner product of eq (1.4) with $\tilde{h}_{\theta kq}^{(1)}$ from eq (1.8) yields

$$\int_{S(z)} \frac{\partial H_\theta}{\partial z} \tilde{h}_{\theta kq}^{(1)} dS = -j\omega\epsilon \int_{S(z)} \mathbf{a}_\theta E_r \cdot \mathbf{a}_z \times \mathbf{a}_r \tilde{e}_{rkq}^{(1)} dS. \quad (1.17)$$

For the left side

$$\begin{aligned} & \int_{S(z)} \frac{\partial H_\theta}{\partial z} \tilde{h}_{\theta kq}^{(1)} dS = \frac{d}{dz} I_{kq} - \sum_{p=0}^{\infty} I_{kp} \int_{S(z)} \{\mathbf{a}_z \times \mathbf{a}_r \tilde{e}_{rkp}^{(1)}\} \\ & \frac{d}{dz} \left\{ \mathbf{a}_z \times \mathbf{a}_r \tilde{e}_{rkq}^{(1)} \right\} dS - \phi_L \tan\{\phi_b(z)\} H_\theta \tilde{h}_{\theta kq}^{(1)} dS \\ & + \phi_L \tan\{\phi_a(z)\} H_\theta \tilde{h}_{\theta kq}^{(1)} dS. \end{aligned} \quad (1.18)$$

Since integration by parts obtains the relation

$$\int_{S(z)} e_{rkp}^{(1)} \frac{d}{dz} \tilde{e}_{rkq}^{(1)} dS = - \int_{S(z)} \tilde{e}_{rkq}^{(1)} \frac{d}{dz} e_{rkp}^{(1)} dS, \quad (1.19)$$

eq (1.17) takes on the form (setting $k=q=0$)

$$\begin{aligned} & \frac{dI_{00}}{dz} = -j\omega\epsilon V_{00}(z) - 2\pi \sum_{p=0}^{\infty} I_{0p}(z) \int_{S(z)} \tilde{e}_{rkq}^{(1)} \frac{d}{dz} e_{rkp}^{(1)} dS \\ & + b'(z) \phi_L H_\theta \tilde{h}_{\theta 00}^{(1)} dS - a'(z) \phi_L H_\theta \tilde{h}_{\theta 00}^{(1)} dS. \end{aligned} \quad (1.20)$$

Substituting eqs (1.6) and (1.10) into eq (1.20) gives

$$\begin{aligned} & \frac{dI_{00}^{(1)}}{dz} + 2\pi \sum_{p=0}^{\infty} I_{0p}^{(1)}(z) \int_{a(z)}^{b(z)} \frac{\tilde{f}_{00}(r, z)}{\tilde{N}_{00}(z)} \frac{\partial}{\partial z} \frac{f_{0p}(r, z)}{N_{0p}(z)} r dr \\ &= -j\omega\epsilon V_{00}^{(1)}(z) \\ & + 2\pi b'(z) \frac{\tilde{f}_{00}[b(z), z]}{\tilde{N}_{00}(z)} b(z) \sum_{p=0}^{\infty} I_{0p}^{(1)}(z) \frac{f_{0p}[b(z), z]}{N_{0p}(z)} \\ & - 2\pi a'(z) \frac{\tilde{f}_{00}[a(z), z]}{\tilde{N}_{00}(z)} a(z) \sum_{p=0}^{\infty} I_{0p}^{(1)}(z) \frac{f_{0p}[a(z), z]}{N_{0p}(z)}. \end{aligned} \quad (1.21)$$

Examining eqs (1.16) and (1.21) reveals that continuous mode coupling occurs through the voltage and current transfer coefficients (left side), respectively, a phenomenon observed by Schelkunoff [7]. Skin effect coupling on the conductor surfaces was also reported by Schelkunoff and Gallawa [10]. When the air line is operated at frequencies appropriate to the principal mode, all TM modes attenuate rapidly below their cutoff frequencies. Consequently, dominant coupling occurs between the forward and backward waves of the principal mode.² In this regard, eq (1.16) assumes the form

$$\begin{aligned} \frac{dV_{00}}{dz} - 2\pi \left\{ \int_{a(z)}^{b(z)} \frac{1}{\left[2\pi \ln \frac{b(z)}{a(z)}\right]^{1/2}} \frac{1}{r} \frac{\partial}{\partial r} \right. \\ \left. \frac{1}{\left[2\pi \ln \frac{b(z)}{a(z)}\right]^{1/2}} r \, dr \right\} V_{00}(z) = -j\omega\mu I_{00}(z) \\ - Z_s \left\{ K[\phi_b(z)] \frac{1}{b(z) \ln \frac{b(z)}{a(z)}} \right. \\ \left. + K[\phi_a(z)] \frac{1}{a(z) \ln \frac{b(z)}{a(z)}} \right\} I_{00}(z) \\ + \left\{ \frac{b'(z)}{b(z) \ln \frac{b(z)}{a(z)}} - \frac{a'(z)}{b(z) \ln \frac{b(z)}{a(z)}} \right\} V_{00}(z), \quad (1.22) \end{aligned}$$

where the superscript, (1), has been dropped since only one mode is involved. Rearranging terms produces the expression

$$\frac{dV_{00}}{dz} + \{j\omega\mu + Z_s \kappa(z)\} I_{00} = T_{00}^{(v)}(z) V_{00}, \quad (1.23)$$

where

$$\kappa(z) = \frac{K[\phi_b(z)]}{b(z)} + \frac{K[\phi_a(z)]}{a(z)} \frac{1}{\ln \frac{b(z)}{a(z)}}, \quad (1.24)$$

$$T_{00}^{(v)}(z) = \frac{1}{2} \left\{ \frac{b'(z)}{b(z)} - \frac{a'(z)}{a(z)} \right\} \frac{1}{\ln \frac{b(z)}{a(z)}}. \quad (1.25)$$

The equation for current proceeds similarly. Equation (1.20) yields

$$\frac{dI_{00}}{dz} = -j\omega\epsilon V_{00} + T_{00}^{(i)}(z) I_{00} \quad (1.26)$$

where the current transfer coefficient is defined as

$$T_{00}^{(i)}(z) = \frac{3}{2} \left\{ \frac{b'(z)}{b(z) \ln \frac{b(z)}{a(z)}} - \frac{a'(z)}{a(z) \ln \frac{b(z)}{a(z)}} \right\}. \quad (1.27)$$

3. Conversion of Generalized Telegraphist Equations to Forward and Backward Wave Equations

Following Solymar [9] we define the amplitudes of the forward and backward waves A_{00}^{\dagger} and $A_{00}^{\bar{\dagger}}$ from the relations

$$V_{00} = k_0^{1/2} \{A_{00}^{\dagger} + A_{00}^{\bar{\dagger}}\},$$

$$I_{00} = k_0^{-1/2} \{A_{00}^{\dagger} - A_{00}^{\bar{\dagger}}\},$$

where $k_0 = \mu/\epsilon$, the wave impedance. Substituting eq (2.1) into eqs (1.4) and (1.20) produces the expression

$$\begin{aligned} \frac{dA_{00}^{\dagger}}{dz} + \left\{ j\beta + \frac{Z_s \kappa(z)}{2k_0} \right\} A_{00}^{\dagger} = T_{00}(z) A_{00}^{\dagger} \\ - \frac{Z_s \kappa(z)}{2k_0} A_{00}^{\bar{\dagger}} - \frac{1}{2} T_{00}(z) A_{00}^{\bar{\dagger}}, \quad (2.2) \end{aligned}$$

$$\begin{aligned} \frac{dA_{00}^{\bar{\dagger}}}{dz} - \left\{ j\beta + \frac{Z_s \kappa(z)}{2k_0} \right\} A_{00}^{\bar{\dagger}} = T_{00}(z) A_{00}^{\bar{\dagger}} \\ - \frac{Z_s \kappa(z)}{2k_0} A_{00}^{\dagger} - \frac{1}{2} T_{00}(z) A_{00}^{\dagger}, \quad (2.3) \end{aligned}$$

where $\beta = \omega\sqrt{\mu\epsilon}$,

$$T_{00}(z) = \frac{1}{2} \{T_{00}^{(v)}(z) + T_{00}^{(i)}(z)\}. \quad (2.4)$$

In view of eqs (1.25) and (1.27) the last expression possesses the form

$$T_{00}(z) = \frac{1}{\ln \frac{b(z)}{a(z)}} \left\{ \frac{b'(z)}{b(z)} - \frac{a'(z)}{a(z)} \right\}. \quad (2.5)$$

For a lossless airline, voltage and current transfer coefficients assume the form,

$$-T_{00}^{(v)}(z) = T_{00}^{(i)}(z) = \frac{1}{2} \frac{1}{\ln \frac{b(z)}{a(z)}} \left\{ \frac{b'(z)}{b(z)} - \frac{a'(z)}{a(z)} \right\}. \quad (2.6)$$

² Higher order mode influence on the TEM mode will be reported in a later issue of this journal.

Also, using Solymar's assumption that reflection of the principal mode does not affect forward propagation of the principal mode yields expressions

$$\frac{dA_{00}^+}{dz} + j\beta A_{00}^+ = 0, \quad (2.7a)$$

and

$$\frac{dA_{00}^+}{dz} - j\beta A_{00}^- = -\frac{1}{2} \frac{1}{\ln \frac{b(z)}{a(z)}} \left\{ \frac{b'(z)}{b(z)} - \frac{a'(z)}{a(z)} \right\}, \quad (2.7b)$$

which agree with Hill's results [5].

Returning to eqs (2.2) and (2.3) and retaining Solymar's assumption above leaves the terms $T_{00}(z) A_{00}^\pm$. Since coupling in this sense is meaningless, we drop the terms $T_{00}(z) A_{00}^\pm$ and obtain³

$$\frac{dA_{00}^+}{dz} + \left\{ j\beta + \frac{Z_s \kappa(z)}{2k_0} \right\} A_{00}^+ = 0, \quad (2.8)$$

$$\frac{dA_{00}^-}{dz} - \left\{ j\beta + \frac{Z_s \kappa(z)}{2k_0} \right\} A_{00}^- = \left\{ \frac{Z_s \kappa(z)}{2k_0} + \frac{T_{00}(z)}{2} \right\} A_{00}^+. \quad (2.9)$$

To incorporate appropriate boundary conditions, let the incident wave be $A_{00}^+(0) = A_0$ with perfect termination at $z = L$, that is $A_{00}^-(L) = 0$.

At this point the forward wave solution yields

$$A_{00}^+(z) = -A_0 e^{-\int_0^z \left\{ j\beta + \frac{Z_s \kappa(\xi)}{2k_0} \right\} d\xi}, 0 \leq z \leq L \quad (2.10)$$

and, at $z = 0$, the reflected wave expression

$$A_{00}^-(0) = -A_0 \int_0^L \left\{ \frac{Z_s \kappa(z)}{2k_0} + \frac{T_{00}(z)}{2} \right\} e^{-2\int_0^z \left\{ j\beta + \frac{Z_s \kappa(\xi)}{2k_0} \right\} d\xi} dz \quad (2.11)$$

show general forms which remain to be useful for using conductor radii measurements.

From eqs. (2.6) and (2.7) the scattering parameters S_{11} and S_{21} are defined as follows:

$$S_{11} = \frac{A_{00}^-(0)}{A_0} \text{ and } S_{21} = \frac{A_{00}^+(L)}{A_0}. \quad (2.12)$$

³ In the lossless air line $T_{00}(z) = 0$ in view of the eqs (2.5) and (2.6).

4. Cubic Spline Fitting of Conductor Radius Measurements

Underlying an accurate solution to A_{00}^+ and A_{00}^- are two critical items: (a) fitting conductor radii measurements with acceptable error bounds and (b) expansion of all known functions in a systematic manner to sufficient powers of z .

To handle (a) consider cubic spline polynomials [13] for the inner (or outer) conductor measurements such that

$$\hat{C}_{k-1}(z) = \hat{C}_{0,k-1} + \dots + \hat{C}_{3,k-1} z^3 \quad (3.1)$$

where $\hat{C}_{k-1}(z)$ approximates $a(z)$ or $b(z)$, $z_{k-1} \leq z \leq z_k$ such that $k = 1, \dots, N$ and $z_N = L$. It is desirable to transform the cubic spline eq (3.1) over the interval $[z_{k-1}, z_k]$ into the representation⁴

$$C_{k-1}(\xi) = C_{0,k-1} + \dots + C_{3,k-1} \xi^3, \quad (3.2a)$$

in such a way that the condition,

$$\frac{d^2 C_{k-1}(\xi)}{d\xi^2} = \frac{d^2 \hat{C}_{k-1}(z)}{dz^2}, \quad (3.2b)$$

holds at $z = z_{k-1}$ and $z = z_k$ where $\xi = z_k - z_{k-1}$. In addition we require

$$C_{k-1}(0) = \hat{C}_{0,k-1}, \text{ and}$$

$$C_{k-1}(z_k - z_{k-1}) = \hat{C}_{0,k-1} + \dots + \hat{C}_{3,k-1} z_k^3 \quad (3.2c)$$

such that $\hat{C}_{0,k-1}$ represents the measurement of $a(z)$ or $b(z)$ at $z = z_{k-1}$.

To implement (b), recall that E_r , H_θ , and the second derivatives of E_r and H_θ are assumed to be analytic functions in r , θ , and z . Hence, the expansions of $\left\{ b(z) \ln \frac{b(z)}{a(z)} \right\}^{-1}$ and $\left\{ a(z) \ln \frac{b(z)}{a(z)} \right\}^{-1}$ can be rearranged in powers of z . In Appendix C the following expressions are derived over the interval $[z_{m-1}, z_m]$:

$$j\beta + \frac{Z_s \kappa(\xi)}{2k_0} = \sum_{k=0}^3 \delta_{k,m-1}^{(q)} \xi^k, \quad (3.3)$$

and

⁴ A cursory inspection of calculated splines C_k over the entire length of the line reveals that \hat{C}_{0k} is not necessarily equal to the radial measurement at z_{k-1} .

$$\frac{Z_s \kappa(\zeta)}{2k_0} + \frac{T_{00}(\zeta)}{2} = \sum_{k=0}^3 \delta_{k,m-1}^{(2)} \zeta^k, \quad (3.4)$$

where $0 \leq \zeta \leq z - z_{m-1}$.

To establish A_{00}^- and A_{00}^+ at each point z_n it is convenient to employ recursion relations. Inserting eq (3.3) into eq (2.6) and examining the interval $z_1 \leq z \leq z_2$ yields

$$A_{00}^+(0; z) = A_{00}^+(0; z_1) e^{-\int_0^{z-z_1} \sum_{k=0}^3 \delta_{k,1}^{(1)} \zeta^k d\zeta} \quad (3.5)$$

where

$$A_{00}^+(0; z_1) = A_0 e^{-\int_0^{z_1} \sum_{k=0}^3 \delta_{k,0}^{(1)} \zeta^k d\zeta} \quad (3.6)$$

is the forward wave emerging at $z = z_1$.

For the interval $z_{N-1} \leq z \leq z_2$ eq (3.5) immediately generalizes to the recursion relation

$$A_{00}^+(0; z) = A_{00}^+(0; z_{N-1}) e^{-\int_0^{z-z_{N-1}} \sum_{k=0}^3 \delta_{k,N-1}^{(1)} \zeta^k d\zeta}. \quad (3.7)$$

Proceeding to the backward wave A_{00}^- by using eqs (3.3) and (3.4) in eq (2.7) for the interval $z_1 \leq z \leq z_2$ produces the relation

$$A_{00}^-(0; z) = A_{00}^-(0; z_1) - A_{00}^+(0; z_1) \{ e^{-j\beta z_1} \int_0^{z_2-z_1} \sum_{k=0}^3 \delta_{k,1}^{(2)} \eta^k \cdot e^{-2\int_0^\eta \sum_{k=0}^3 \delta_{k,1}^{(1)} \zeta^k d\zeta} d\eta \} \quad (3.8)$$

where the transformation $\eta = z - z_1$ introduces the term $e^{-j\beta z_1}$. Now eq (3.8) also generalizes to the recursion relation

$$A_{00}^-(0; z_N) = A_{00}^-(0; z_{N-1}) - A_{00}^+(0; z_{N-1}) e^{-j\beta z_{N-1}} \int_0^{z_N-z_{N-1}} \sum_{k=0}^3 \delta_{k,N-1}^{(2)} \eta^k \cdot \{ e^{-2\int_0^\eta \sum_{k=0}^3 \delta_{k,N-1}^{(1)} \zeta^k d\zeta} \} d\eta. \quad (3.9)$$

From Appendix C eq (3.9) assumes the solution

$$A_{00}^-(0; z_N) = A_{00}^-(0; z_{N-1}) - A_{00}^+(0; z_{N-1}) e^{-j\beta z_{N-1}} \cdot \sum_{k=0}^3 \nu_{k,N-1}^{(2)} S_k \left\{ - \left[2j\beta + \frac{Z_s}{k_0} C_{0,N-1}^{(2)} \right] (z_N - z_{N-1}) \right\}, \quad (3.10)$$

where

$$S_k[\alpha(z_N - z_{N-1})] = \int_{z_{N-1}}^{z_N} e^{\alpha z} z^k dz. \quad (3.11)$$

5. Conductor Surface Variations in the Transverse Coordinates

When the outer conductor is bored, circular cross sections are the exception rather than the rule. Most likely, an elliptical cross section evolves with some degree of rotation. Consequently, it is desirable to perform mechanical measurements of conductor radii in the transverse plane to characterize the deviation from circular cross sections. Since the principal mode is TEM in the transverse plane a direct conformal mapping of the measurement contour into an equivalent circular contour eliminates any difficulty of solving Laplace's equation for an irregular boundary. If an equivalent circular contour is found for each transverse measurement plane on the air line, a corresponding set of scattering parameters represents the original air line of measurement contours.

The solution of Laplace's equation for a TEM mode with the inner conductor potential held to V_0 and the outer conductor potential set at 0 is

$$\phi = V_0 \frac{\ln\{r/b(z)\}}{\ln\{a(z)/b(z)\}}. \quad (4.1)$$

We initially state that Riemann's mapping theorem assures a mapping from the contour L to the unit circle and a particular expression for mapping evolves from the Bergman kernel expansion [14]. Thus, for a contour L centered at $\zeta_0 = \delta e^{i\theta} = 0$ the Bergman kernel is defined as

$$B(0, \zeta) = \sum_{\nu=0}^{\infty} P_{\nu}^{-} (0) P_{\nu}(\zeta). \quad (4.2)$$

The Szegő polynomials $P_{\nu}(\zeta)$ are constructed to be orthogonal on the contour L and ζ is a complex variable in the region bounded by L . Computing the inner (or outer) conductor radius requires the expression [15]

$$c(z) = \frac{\ell_0(z)}{2\pi} \cdot \frac{1}{B(0,0)}, \quad c(z) = a(z) \text{ or } b(z), \quad (4.3)$$

where ℓ defines the contour length of L at the point z . To see how eq (4.3) is constructed consider the differential line element on L ,

$$ds^2 = dx^2 + dy^2,$$

which in ρ, θ coordinates becomes

$$ds^2 = \left\{ \rho^2(\theta) + \left[\frac{\partial \rho}{\partial \theta} \right]^2 \right\} d\theta^2. \quad (4.4)$$

Then the length of L is

$$\ell_0 = \int_0^{2\pi} ds = \int_0^{2\pi} \left\{ \rho^2(\theta) + \left[\frac{\partial \rho}{\partial \theta} \right]^2 \right\}^{1/2} d\theta. \quad (4.5)$$

To find representations for the Szegő polynomials, consider the following orthogonalization procedure. Let the matrix elements,

$$h_{pq} = \frac{1}{\ell_0} \int_L \zeta^p \bar{\zeta}^q ds = \frac{1}{\ell_0} \int_0^{2\pi} \rho^{p+q}(\theta) \left\{ \rho^2(\theta) + \left[\frac{\partial \rho}{\partial \theta} \right]^2 \right\}^{1/2} e^{i(p-q)\theta} d\theta, \quad (4.6)$$

be defined for $p \geq 0$ and $q \geq 0$. Note $\bar{h}_{pq} = h_{qp}$. Then following Kantorovich and Krylov [15] compute the determinant

$$D_0 = 1, D_n = \begin{vmatrix} h_{00} & h_{10} & \dots & h_{n0} \\ \vdots & \vdots & \dots & \vdots \\ h_{0n} & h_{1n} & \dots & h_{nn} \end{vmatrix}. \quad (4.7)$$

Hence, the Szegő polynomial is defined as

$$P_n(\zeta) = \frac{1}{[D_{n-1}D_n]^{1/2}} \begin{vmatrix} h_{00} & h_{10} & \dots & h_{n0} \\ h_{01} & h_{11} & \dots & h_{n1} \\ \vdots & \vdots & \dots & \vdots \\ h_{0,n-1} & h_{1,n-1} & \dots & h_{n,n-1} \\ 1 & z & \dots & z^n \end{vmatrix}, \quad (4.8)$$

such that

$$\frac{1}{\ell_0} \oint_L P_n(\zeta) \bar{P}_m(\bar{\zeta}) d\zeta = \delta_{nm}. \quad (4.9a)$$

Carrying out the above procedures yields the conductor radii accurate to third order,

$$C = \frac{\ell_0}{2\pi} \left\{ 1 - \frac{\bar{h}_{10} h_{10}}{D_1 \bar{D}_1} - \frac{(\bar{h}_{10} \bar{h}_{21} - \bar{h}_{11} \bar{h}_{20})(h_{10} h_{21} - h_{11} h_{20})}{D_1 \bar{D}_2 \bar{D}_1 D_2} \right\}, \quad (4.9b)$$

where

$$D_1 = h_{11} - h_{01} h_{10},$$

and

$$D_2 = (h_{11} h_{22} - h_{12} h_{21}) - h_{10} (h_{01} h_{22} - h_{02} h_{21}) + h_{20} (h_{01} h_{12} - h_{02} h_{11}). \quad (4.10)$$

A convenient property of the Szegő coefficients for symmetric contours is found from eq (4.6). We have

$$h_{pq} = \frac{1}{\ell_0} \int_0^{2\pi} \left\{ 1 + (-1)^{p+q}(\theta) \left\{ \rho^2(\theta) + \left[\frac{\partial \rho}{\partial \theta} \right]^2 \right\}^{1/2} e^{i(p-q)\theta} d\theta. \right.$$

For off diagonal elements

$$h_{pq} = 0; p+q \text{ odd}, p \neq q.$$

Hence, any asymmetry in the contour L is expected to be noticeable through the off-diagonal elements h_{pq} .

To find the equivalent circular conductor radius, integrals in eqs (4.5) and (4.6) need to be determined from measurements of ρ and θ on the contour L . Let the following cubic spline be defined

$$\hat{\rho}_{k-1}(\theta) = \sum_{i=0}^3 \hat{\rho}_{i,k-1} \theta^i \quad (4.11a)$$

such that $\hat{\rho}_{k-1}(\theta)$ approximates $a(\theta, z)$ or $b(\theta, z)$ over the interval $\theta_{k-1} \leq \theta \leq \theta_k$ for $k=1, \dots, N$, i.e., $\theta_N = 2\pi$.

Following the same procedures as in the transformation from z to ζ in eqs (3.2a) to (3.2c) enables the cubic spline,

$$\rho_{k-1}(\phi) = \sum_{i=0}^3 (\rho_{i,k-1}) \phi^i, \quad (4.11b)$$

to be constructed where $\Phi = \theta - \theta_{k-1}$ and $\rho_{0,k-1}$ equals the measurement of $a(\theta, z)$ or $b(\theta, z)$ at $\theta = \theta_{k-1}$.

Equations (4.5) and (4.11) yield an expression for length using the binomial expansion:

$$\ell_0 = \int_0^{2\pi} \left\{ \rho(\theta) + \frac{1}{2} \rho^{-2}(\theta) \left[\frac{\partial \rho}{\partial \theta} \right]^2 - \dots \right\} d\theta. \quad (4.12)$$

Appendix D, taking into account the spline coefficients, produces

$$\ell_0 = \sum_{n=0}^{N-1} \int_0^{\theta_{n+1} - \theta_n} \left\{ \sum_{k=0}^3 P_{1,k,n}^{(1)} \theta^k + \frac{1}{2} \sum_{k=0}^7 P_{2,k,n}^{(1)} \theta^k \right\} d\theta, \quad (4.13)$$

$$\ell_0 = \sum_{n=0}^{N-1} \left\{ \sum_{k=0}^3 P_{1,k,n}^{(1)} \frac{[\theta_{n+1} - \theta_n]^{k+1}}{k+1} + \frac{1}{2} \sum_{k=0}^7 P_{2,k,n}^{(1)} \frac{[\theta_{n+1} - \theta_n]^{k+1}}{k+1} \right\}.$$

Expressions for the coefficients h_{pq} are developed also in Appendix D.

6. Computation Results

The amplitude of S_{11} has been computed from eqs (2.12) and (3.9) for a 7 mm air line approximately 15.6 cm in length using the frequencies 6, 12, and 18 GHz. In addition the number of conductor dimensional measurements in three sections of air line with variable spacing is shown in figure 2 and the results are illustrated in figures 2-5. Mean and standard deviation values of the conductor dimensional measurements are as follows:

	Inner radius	Outer radius
Mean (meters)	0.1521×10^{-2}	0.3500×10^{-2}
Standard deviation (meters)	0.2481×10^{-6}	0.6836×10^{-6}

Figure 2 illustrates that conductor radius measurements near either end are more volatile—particularly the outer conductor. Figures 3, 4, and 5 reveal

that changes in conductor radii in the z-axis provide the dominant contribution to $|S_{11}|$ while skin effect loss amplifies the in-phase and out-of-phase behavior of the lossless air line (as shown in fig. 2). In addition, skin effect loss affects the most significant digit of $|S_{11}|$ even for short lengths of line. On comparison of figures 3, 4, and 5 with Hill's results [5], the most noticeable feature is the overall difference in magnitudes of S_{11} , which evolves from a uniform inner conductor model and lossless boundary conditions in Hill's work. Conformal mapping effects from elliptical measurement contours do not affect S_{11} and S_{21} unless the eccentricity is greater than 5×10^{-6} meters. However, if the inner conductor has an eccentric position with respect to the outer conductor, conformal mapping by Bergman's kernel reveals scattering parameters S_{11} and S_{21} are noticeably affected.⁵

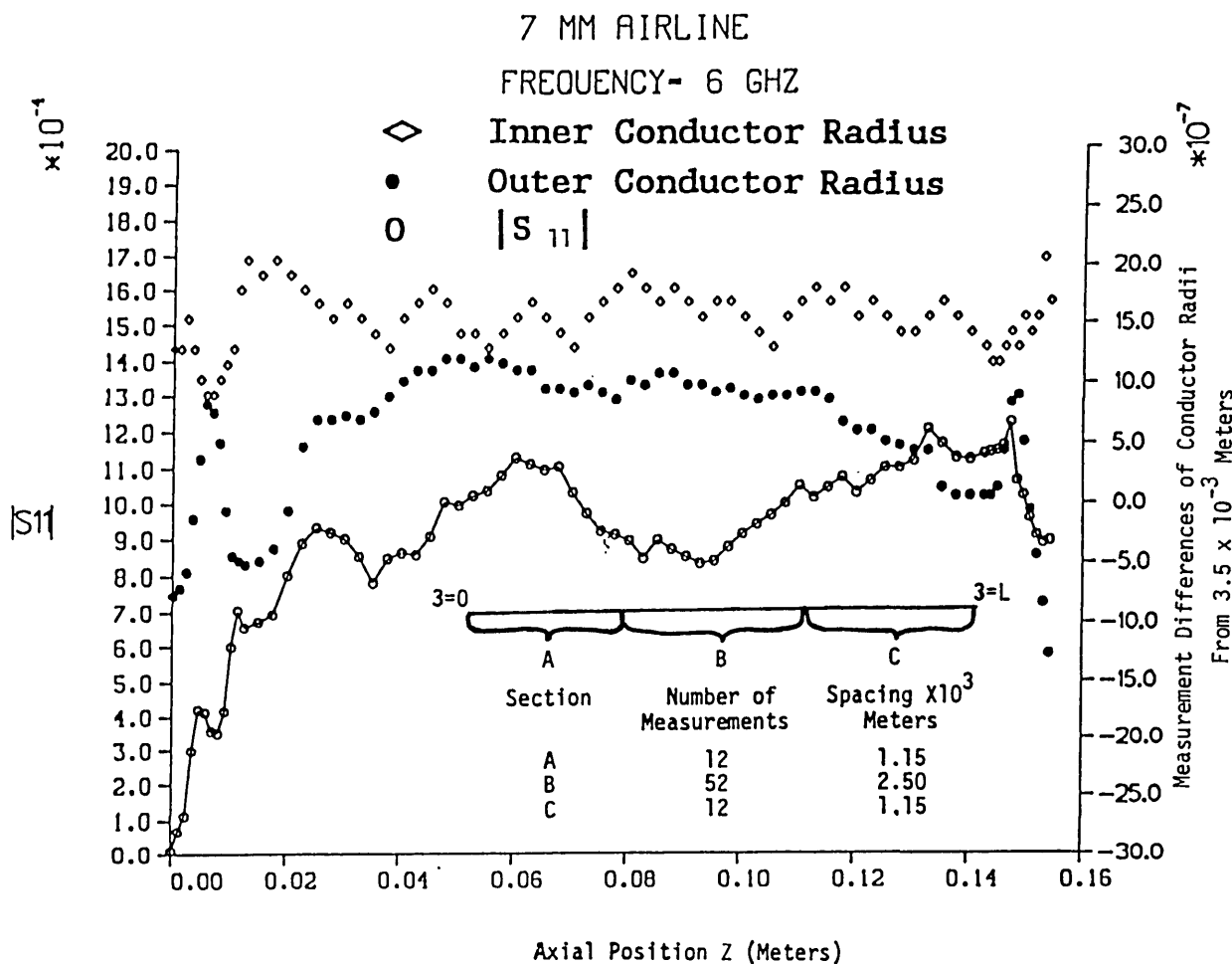


Figure 2. $|S_{11}|$ vs variable length of 7 mm lossless air line.

⁵ For additional computational results see Holt [17].

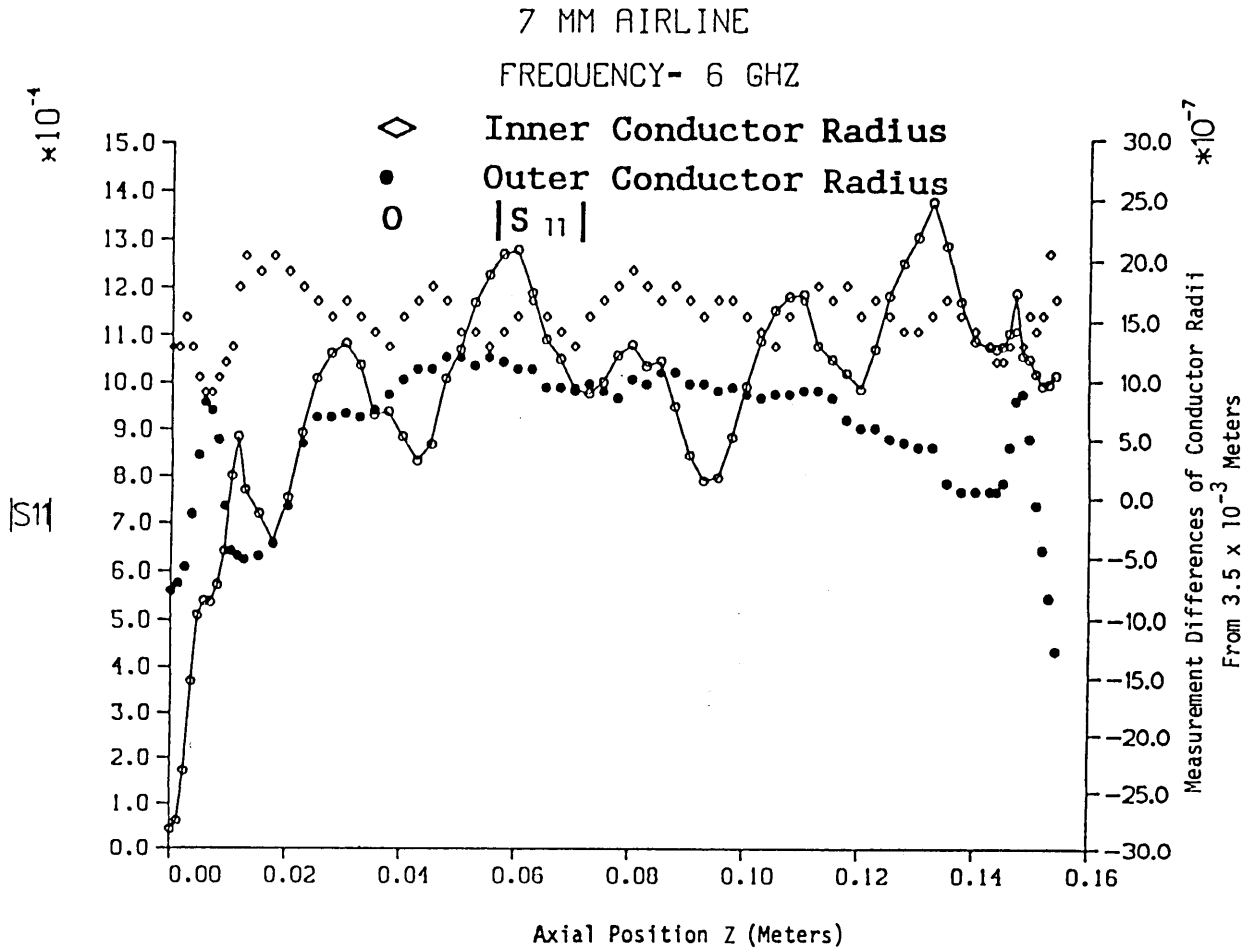


Figure 3. $|S_{11}|$ vs variable length of 7 mm air line with skin effect loss at 6 GHz.

7. Error Analysis

7.1 Error Sources

Error sources that contribute to scattering parameters evolve from (a) spline interpolation with respect to z , (b) spline interpolation with respect to θ , (c) conformal mapping using the Bergman kernel, and (d) expressions for backward and forward waves.

To examine (a) and (b) consider the error bound from cubic spline interpolation theory [13],

$$|f(x) - S\Delta_k(x)| \leq \frac{5}{2} [\Delta_k^2 \mu(f''(x); |\Delta_k|)], \quad (6.1)$$

where $S\Delta_k(x)$ defines a cubic spline, μ signifies the modulus of continuity,⁶ f'' denotes the second derivative of the function f , and Δ_k stands for the mesh size between arguments x_k . An approxima-

tion to the modulus of continuity is

$$\mu[f''(x); |\Delta_k|] = \max \left| \frac{f[x_{k-1}, x_k]}{h} - \frac{f[x_{k+1}, x_k]}{h} \right|, \quad (6.2)$$

where $f[\]$ denotes the first order divided difference of f .

For a 7 mm air line with a mesh size (Δ_k) equal to 1 mm, a value of μ from observations of conductor radii measurements as functions of z indicate $\mu = 0.1$ is reasonable, and in the angular direction $\mu < 0.01$.⁷ Therefore, the total error from spline interpolation is (considering the errors as additive)

$$\text{Error}_{\text{total}} = \text{Error}_z + \text{Error}_\theta < 2.8 \times 10^{-7} \text{ m}. \quad (6.3)$$

⁷ Since mechanical measurements for roundness are not available, an ellipse of 38.1×10^{-6} m was selected for determining the modulus of continuity.

⁶ See Davis [16] for a suitable definition.

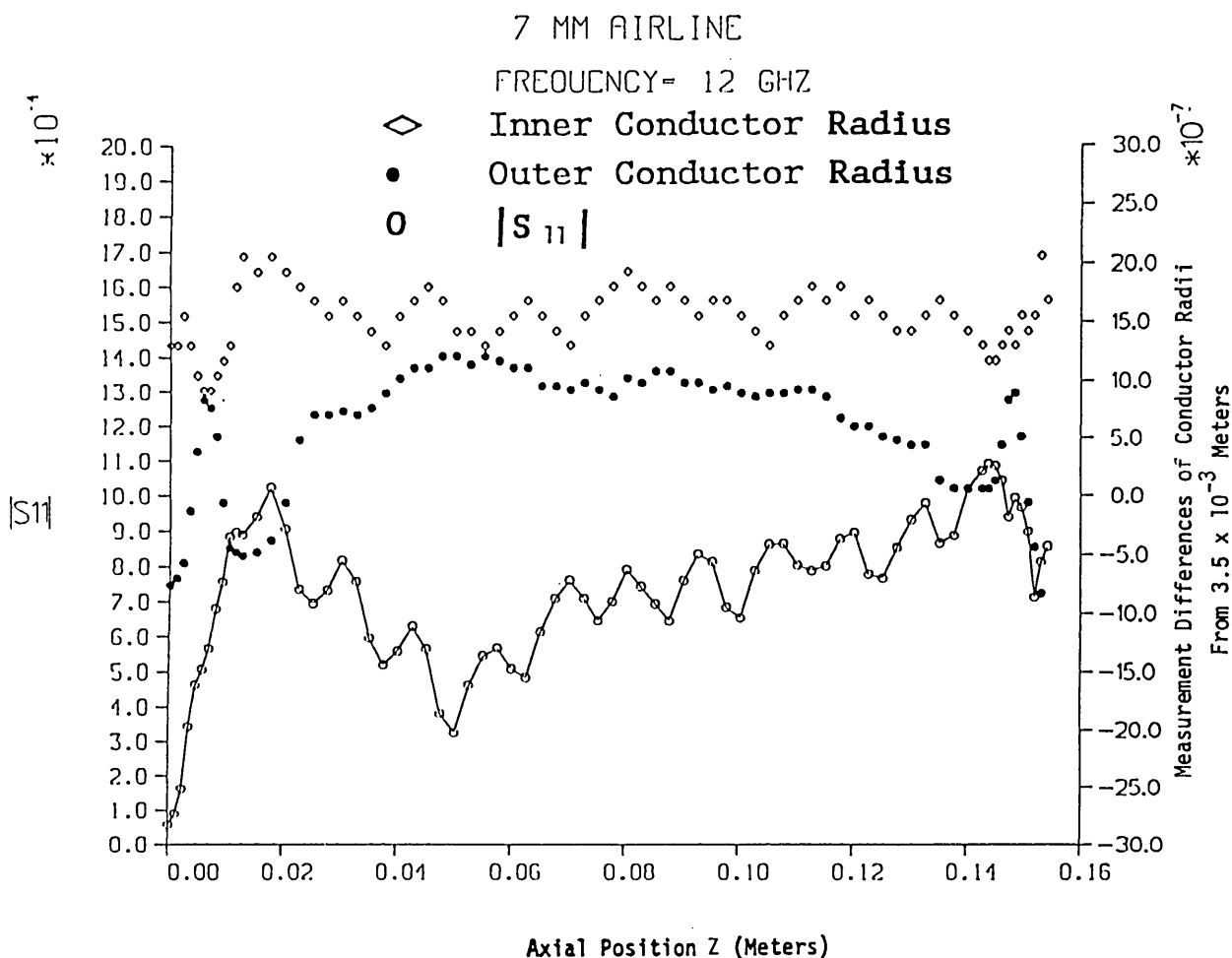


Figure 4. $|S_{11}|$ vs variable length of 7 mm air line with skin effect loss at 12 GHz.

The error source (c) from conformal mapping an elliptical measurement contour of eccentricity equal to 38.1×10^{-6} m (150 μ in) is illustrated below.

First term of outer conductor equivalent (mapped radius) 3.4989 mm.

Second term 2.32×10^{-12} mm.

Third term -3.35×10^{-5} mm.

Keeping in mind that ellipses are symmetrical with respect to the origin reveals that even terms are effectively zero (on the order of 10^{-12} in view of machine precision). Since the convergence above is very strong, the fifth term is likely on the order of 10^{-9} mm. The error from source (d) depends on the number of expansion terms representing the functions $1/a(z)$, $1/b(z)$, and $\ln\{b(z)/a(z)\}$.

At this point accuracy considerations of the forward and backward wave eqs (3.7) and (3.10) in correspondence to the measurement system are in order. For instance, to examine A_{00}^{\pm} consider the measurements of $a(z)$ and $b(z)$ at $z=0$ and $z=z_1$. From eqs (3.7) and (3.10) we have the total differentials

$$\Delta A_{00}^{\pm}(0; z_1) = A_0 \left\{ W(a_0, b_0, Z_s) - \left[\frac{Z_s}{2k_0} U_{2,1}(a_0, b_0) - \frac{Z_s}{2k_0} U_{1,2}(a_0, b_0) \left[\frac{1}{a_0} + \frac{1}{b_0} \right] \right] \right\} e^{-W(a_0, b_0, Z_s) z_1} \Delta r_0 \quad (6.4)$$

and

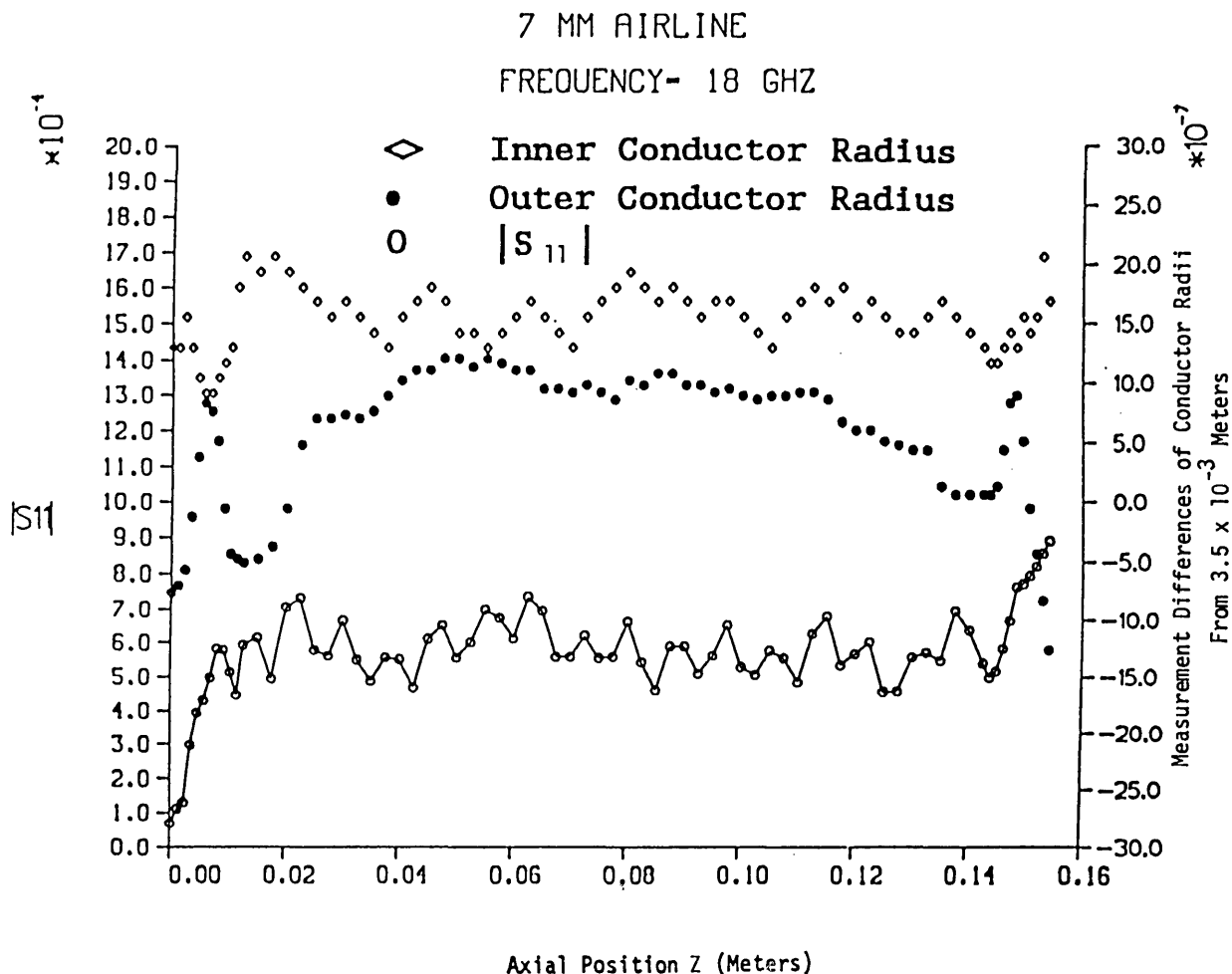


Figure 5. $|S_{11}|$ vs variable length of 7 mm air line with skin effect loss at 18 GHz.

$$\Delta A_{\infty}(0; z_1) = -A_0 \left\{ \frac{Z_s}{2k_0} U_{1,1}(a_0, b_0) + \frac{1}{\ln \frac{b_1}{a_0}} \left[\frac{b_1}{b_0} - \frac{a_1}{a_0} \right] \right\}$$

$$\cdot e^{-2W(a_0, b_0, z_1) z_1} \Delta z_1 + A_0 \frac{Z_s}{2k_0} \left\{ U_{1,1}(a_0, b_0) \left[\frac{b_1}{b_0} - \frac{a_1}{a_0} \right] \right.$$

$$\left. + \frac{1}{\ln \left[\frac{b_0}{a_0} \right]} \left[\frac{a_1}{a_0^2} - \frac{b_1}{b_0^2} \right] \right\} \cdot \frac{e^{-2W(a_0, b_0, Z_s) Z_s} - 1}{2W(a_0, b_0, Z_s)} \Delta r_0$$

$$+ A_0 \frac{Z_s}{2k_0} \{ U_{1,1}(a_0, b_0)$$

$$+ \frac{1}{\ln \left[\frac{b_0}{a_0} \right]} \left[\frac{b_1}{b_0} - \frac{a_1}{a_0} \right] \} \{ U_{2,1}(a_0, b_0)$$

$$- U_{1,2}(a_0, b_0) \left[\frac{1}{a_0} + \frac{1}{b_0} \right] \} \left\{ \frac{1}{W^2(a_0, b_0, Z_s)} \right.$$

$$\left. - \left[\frac{z_1}{W(a_0, b_0, Z_s)} + \frac{1}{W^2(a_0, b_0, Z_s)} e^{-W(a_0, b_0, Z_s) z_1} \right] \right\} \Delta r_0 \quad (6.5)$$

where Δr_0 is the measurement precision common to a_0 and b_0 . In the expressions above

$$U_{\ell, k}(a_0, b_0) = \frac{1}{a_0^\ell} + \frac{1}{b_0^\ell} \frac{1}{\ln k \left[\frac{b_0}{a_0} \right]} \quad (6.6)$$

and

$$W(a_0, b_0, Z_s) = \frac{Z_s}{2k_0} U_{1,1}(a_0, b_0) + \left[\frac{b_1}{b_0} - \frac{a_1}{a_0} \right] \quad (6.7)$$

where a_1 and b_1 are the coefficients from differentiating the cubic spline representations of $a(z)$ and $b(z)$, respectively.

In computing ΔA_{∞}^+ and ΔA_{∞}^- for a 7 mm air line let the measurement precision be $\Delta z = \Delta r_0 = 2.8 \times 10^{-7}$ m for a frequency range of 1-18 GHz. Using the measurements of $a(z)$ and $b(z)$ in figure 3, we select the maximum divided

difference magnitudes for a_1 and b_1 to obtain the results

$$\begin{aligned} |\Delta A_{00}^{\pm}(0; z_1)| & \doteq 3.6 \times 10^{-5} \text{ at 1 GHz,} \\ & \doteq 1.1 \times 10^{-4} \text{ at 18 GHz,} \end{aligned} \quad (6.8)$$

$$\begin{aligned} |\Delta A_{00}^{\pm}(0; z_1)| & \doteq 4 \times 10^{-8} \text{ at 1 GHz,} \\ & \doteq 1.5 \times 10^{-7} \text{ at 18 GHz.} \end{aligned} \quad (6.9)$$

To examine the total uncertainty in A_{00}^{\pm} over N measurements of $a(z_k)$ and $b(z_k)$ for $k=1, \dots, N$ let ΔA_{00}^{\pm} be represented as

$$\Delta A_{00}^{\pm}(0; z_N) \doteq \sum_{n=1}^N f_n \{a(z_n), b(z_n)\} \Delta A_{00}^{\pm}(z_{n-1}, z_n), \quad (6.10)$$

where f_n is on the order of $A_{00}^{\pm}(z_{n-1}, z_n)$. Since the computation of $\Delta A_{00}^{\pm}(z_{n-1}, z_n)$ proceeds in the same way as $\Delta A_{00}^{\pm}(0; z_1)$, in eq (6.5), the total uncertainty over all measurement positions is found when the individual uncertainties in z and r_0 at each measurement position are known.

7.2 Efficiency Improvements in Cubic Spline Approximation

While fitting the surfaces of coaxial air line geometries with products of cubic splines over the variables θ and z successfully meets error bounds consistent with measurement precision, significant reductions in the number of measurements yields equivalent error bounds with Gordon's successive decomposition spline [18]. The number of measurements required for successive decomposition splines in comparison to usual spline products is generally less than 50 percent.

8. Summary

Generalized telegraphist equations for the coaxial air line have been derived under two assumptions: (a) skin effect losses are present, and (b) conductor surface variations occur in the axial and transverse coordinates. Product cubic spline expressions to accurately fit conductor surface measurements were employed to arrive at pointwise scattering parameter expressions. Error bounds from eqs (6.8) and (6.9) reveal at least four significant figures can be obtained to characterize the scattering parameters S_{21} and S_{11} in correspondence

to a conductor surface measurement resolution of 2.8×10^{-7} m over frequencies appropriate to the principal mode for 7 mm air lines.

9. Acknowledgments

The author expresses sincere appreciation to the following staff members of NIST: (a) B. C. Yates for many helpful and critical comments over the project duration (especially examining the numerical results of $|S_{11}|$); (b) R. L. Jesch for general leadership and advice during the manuscript preparation, and (c) E. G. Johnson for stimulating theoretical discussions on various aspects of air line modeling.

About the author: Donald R. Holt is a mathematician in the Electromagnetic Fields Division of the National Institute of Standards and Technology, Boulder, CO.

10. References

- [1] Stratton, J. A., *Electromagnetic theory*. McGraw-Hill, Inc.: New York (1941) pp. 523-537.
- [2] Rice, S. O., Reflection of electromagnetic waves from slightly rough surfaces. *Comm. Pure Appl. Math.* **4**, 351, (1951).
- [3] Ament, W. S., Towards a theory of reflection by a rough surface. *Proc. IRE* **41**, 142, (1953).
- [4] Karbowiak, A. E., Theory of waveguides: the effect of wall impedance. *Institution of Electrical Engineers IEE Paper No. 1841R* (Sept. 1955) pp. 698-708.
- [5] Hill, D., Reflection coefficient of a waveguide with slightly rough walls. *IEEE MTT* 1988.
- [6] Roumeliotis, J. A., Hossain, A. B., Siddique, M. and Fikioris, J. G., Cutoff wave numbers of eccentric circular and concentric circular-elliptic metallic wave guides. *Radio Sci.* **15**, 923, (1980).
- [7] Schelkunoff, S. A., Conversion of Maxwell's equations into generalized telegraphist's equations. *Bell System Tech. J.* **34**, 995, (1955).
- [8] Reiter, G., Generalized telegraphist's equations for waveguides of varying cross section. *Institution of Electrical Engineers IEE Paper No. 3028E* (Sept. 1959) pp. 54-57.
- [9] Solymar, L., Spurious mode generation in nonuniform waveguide. *IRE Microwave Theory and Techniques MTT-7* (1979) pp. 379-383.
- [10] Gallawa, R. L., Propagation in nonuniform waveguides with impedance walls. *J. Res. Natl. Bur. Stand. (U.S.)* **68**, 1201, (1964).
- [11] Ramo, W., and VanDuzer, Fields and waves in communication electronics. Wiley & Sons: New York (1965) pp. 414-415.
- [12] Carslaw, H. S., *An introduction to the theory of Fourier's series and integrals*. Dover: New York (1930) pp. 269-288.

- [13] Ahlberg, J. H., Nilson, E. N., and Walsh, J. L., The theory of splines and their applications, Chapter 1. Academic Press: New York (1967).
- [14] Nahari, Z., Conformal mapping. McGraw-Hill, Inc.: New York (1952) pp. 173–239.
- [15] Kantorovich, L. V., and Krylov, V. I., Approximate methods of higher analysis. Interscience Publishers: New York (1958) pp. 383–385.
- [16] Davis, P. J., Interpolation and approximation. Blaisdell: New York (1963) pp. 7–8.
- [17] Holt, D. R., Scattering parameters of precision coaxial air line standards. IEEE Trans. Instru. Meas.
- [18] Gordon, W. J., Approximations with special emphasis on spline functions. Academic Press: New York (1969) pp. 269–270.

Appendix A. Inner and Outer Conductor Boundary Conditions

In reference to figure 6 the boundary condition is

$$E_\nu = Z_s J_\nu \tag{A.1}$$

where E_ν is the electric field component, J_ν is the current density component in the coordinate ν , and Z_s is the radial impedance at $r=b(z)$.

Also from figures 1 and 6

$$\mathbf{a}_\nu = |a_\nu| \cos\{\phi_b(z)\} \mathbf{a}_z + |a_\nu| \sin\{\phi_b(z)\} (-\mathbf{n}), \tag{A.2}$$

$$\mathbf{a}_\nu = \cos\{\phi_b(z)\} \mathbf{a}_z - \sin\{\phi_b(z)\} \mathbf{n},$$

where \mathbf{n} is the unit outward normal vector. From the left side of eqs (A.1) and (A.2)

$$E_\nu \mathbf{a}_\nu = |E_\nu| \cos\{\phi_b(z)\} \mathbf{a}_z - |E_\nu| \sin\{\phi_b(z)\} \mathbf{n},$$

$$E_\nu \mathbf{a}_\nu = E_z \mathbf{a}_z + E_r \mathbf{a}_r.$$

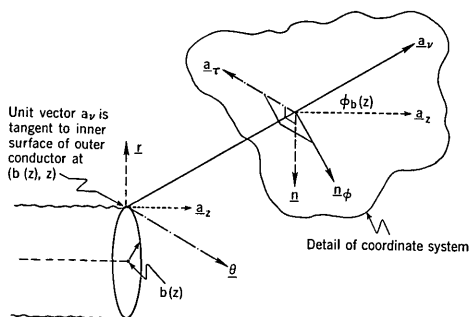


Figure 6. Outer conductor coordinate systems for determining boundary conditions.

Proceeding with the right side of eq (A.1), yields

$$J_\nu \mathbf{a}_\nu = J_z \mathbf{a}_z - J_n \mathbf{n} = \mathbf{a}_z \cdot \mathbf{n} \times \mathbf{H} - J_n \mathbf{n}. \tag{A.4}$$

To find an expression for J_n note that

$$J_n = \mathbf{n} \cdot \mathbf{J}_\nu = \mathbf{n} \cdot \mathbf{n}_\phi \times \mathbf{H}, \tag{A.5}$$

$$J_n = \mathbf{n} \cdot \mathbf{n}_\phi \times \{H_r \mathbf{a}_r + H_n \mathbf{n} + H_z \mathbf{a}_z\},$$

$$J_n = \mathbf{n} \cdot \mathbf{n}_\phi \times \{H_r \mathbf{a}_r + H_n \{-\sin\{\phi_b(z)\} \mathbf{a}_\nu + \cos\{\phi_b(z)\} \mathbf{n}_\phi\}. \tag{A.6}$$

$$+ H_z \{\cos\{\phi_b(z)\} \mathbf{a}_\nu + \sin\{\phi_b(z)\} \mathbf{n}_\phi\},$$

$$J_n = -\sin\{\phi_b(z)\} H_r.$$

Consolidating eqs (A.3), (A.4), and (A.6) yields

$$E_z = -Z_s \left\{ \frac{1 + \sin\{\phi_b(z)\}}{1 + \tan\{\phi_b(z)\}} \right\} H_\theta \tag{A.7}$$

where the relation $E_z \tan\phi(z) = E_r$ has been employed.

The inner conductor boundary condition relation is similarly derived as follows: We have $E_\nu = Z_s J_\nu$ and the left hand side is

$$E_\nu = E_z + E_r. \tag{A.8}$$

The right side becomes

$$\mathbf{a}_\nu J_\nu = \mathbf{a}_z J_z + \mathbf{a}_r J_r. \tag{A.9}$$

Now proceeding as before yields

$$J_r = \mathbf{a}_r \cdot \mathbf{J}_\nu = \mathbf{a}_r \cdot \mathbf{n}_\phi \times \mathbf{H}, \tag{A.10}$$

$$J_r = \mathbf{a}_r \cdot H_\theta \mathbf{a}_\nu,$$

$$J_r = \sin\{\phi_a(z)\} H_\theta. \tag{A.11}$$

Substituting $E_r = \tan\{\phi_a(z)\} E_z$ into eq (A.8) and using eq (A.11) in (A.9) yields

$$E_z = Z_s \left\{ \frac{1 + \sin\{\phi_a(z)\}}{1 + \tan\{\phi_a(z)\}} \right\} H_\theta. \tag{A.12}$$

Appendix B. Transformation of Basis Functions for the Field Components

The transverse fields E_r and H_θ are represented as

$$E_r(r, \theta, z) = \sum_{n,p} \frac{\partial}{\partial r} \Phi_{np}(r, z) \{ \hat{V}_{np}^{(1)}(z) \cos(n\theta) + \hat{V}_{np}^{(2)}(z) \sin(n\theta) \} \quad (B.1)$$

$$H_\theta(r, \theta, z) = \sum_{n,p} \frac{\partial}{\partial r} \Phi_{np}(r, z) \{ \hat{I}_{np}^{(1)}(z) \cos(n\theta) + \hat{I}_{np}^{(2)}(z) \sin(n\theta) \} \quad (B.2)$$

where Φ_{np} denotes the radial component of the normalized potential function at a point, z . The symbol $\hat{}$ over V_{np} (or I_{np}) signifies an amplitude corresponding to the nonorthogonal function $\frac{\partial}{\partial r} \Phi_{np}$ and the superscripts (1) [and (2)] correspond to even and odd modes. We assume that E_r and H_θ have first and second derivatives in r and θ which are continuous and bounded. Hence, the Fourier series eqs (B.1) and (B.2) are absolutely and uniformly convergent; that is the series can be rearranged.

Suppose the k th even mode of eqs (B.1) and (B.2) is considered and let the Gram-Schmidt orthogonalization be represented as

$$\frac{\partial}{\partial r} \Phi_{np}(r, z) = \sum_{\ell=0}^p a_{k,p-1,\ell}(z) f_{k\ell}(r, z) / N_{k\ell}(z) \quad (B.3)$$

where $f_{k\ell}(r, z) / N_{k\ell}(z)$ is the $k\ell$ th orthogonal basis function. Now substituting eq (B.3), multiplying eq (B.1) by $\cos(k\theta)$, and integrating over θ yields

$$\begin{aligned} & \int_0^{2\pi} E_r(r, \theta, z) \cos(k\theta) d\theta \\ &= \{ \hat{V}_{k0}(z) a_{k,0,0}(z) f_{k0}(r, z) / N_{k0}(z) \} \\ &+ \hat{V}_{k1}(z) \{ a_{k,1,0}(z) \frac{f_{k0}(r, z)}{N_{k0}(z)} + a_{k,1,1}(z) \frac{f_{k1}(r, z)}{N_{k1}(z)} \} + \dots \\ &+ \hat{V}_{km}(z) \{ a_{k,m,0}(z) \frac{f_{k0}(r, z)}{N_{k0}(z)} \\ &+ \dots + a_{k,m,m}(z) \frac{f_{km}(r, z)}{N_{km}(z)} \} + \dots \} \nu(k). \quad (B.4) \end{aligned}$$

By induction note that the basis function $f_{k0}(r, z) / N_{k0}(z)$, occurs in every term above. Hence, we set

$$V_{k,0}^{(1)}(z) = \sum_{\ell=0}^{\infty} a_{k,\ell,0}(z) \hat{V}_{k\ell}(z).$$

Proceeding to the m th term yields the expression

$$V_{km}^{(1)}(z) = \sum_{\ell=m}^{\infty} a_{k,\ell,m}(z) \hat{V}_{k\ell}(z) \quad (B.5)$$

for the coefficient of the basis function $f_{km}(r, z) / N_{km}(z)$. Now eq (B.4) from eq (B.5) becomes

$$\begin{aligned} & \int_0^{2\pi} E_r(r, \theta, z) \cos k\theta d\theta \\ &= \nu(k) \sum_{p=0}^{\infty} V_{kp}^{(1)}(z) f_{kp}(r, z) / N_{kp}(z) \quad (B.6) \end{aligned}$$

for the k th even component of E_r . The odd components of E_r are obtained similarly. Hence, summing all components of E_r obtains the desired result

$$E_r(r, \theta, z) = \nu(n) \sum_{n,p} \frac{f_{np}(r, z)}{N_{np}(z)} \{ V_{np}^{(1)}(z) \cos(n\theta) + V_{np}^{(2)}(z) \sin(n\theta) \} \quad (B.7)$$

where $\nu(n) = 2\pi$ if $n = 0$
 $= \pi$ if $n \neq 0$

The expansion for H_θ is obtained in the same way, i.e.,

$$H_\theta(r, \theta, z) = \nu(n) \sum_{n,p} \frac{f_{np}(r, z)}{N_{np}(z)} \{ I_{np}^{(1)}(z) \cos(n\theta) + I_{np}^{(2)}(z) \sin(n\theta) \}. \quad (B.8)$$

Appendix C

Beginning with the spline expressions eq (3.1), consider the reciprocal

$$\frac{1}{b(z)} = \frac{1}{b_0} \frac{1}{1 + \frac{b_1}{b_0} z + \dots + \frac{b_3}{b_0} z^3}. \quad (C.1)$$

We define the coefficients

$$B_1^{(0)} = b_1/b_0, \dots, B_3^{(0)} = b_3/b_0. \quad (C.2)$$

Since the geometric series for small z ,

$$\left| \frac{b_1}{b_0} z + \dots + \frac{b_3}{b_0} z^3 \right| \ll \alpha_0 \ll 1$$

converges uniformly and absolutely, eq (C.1) can be rearranged in powers of z . We have

$$\frac{1}{b(z)} = \frac{1}{b_0} \frac{1}{1 + B_1^{(0)}z + \dots + B_3^{(0)}z^3}.$$

Using the geometric expansion yields

$$\begin{aligned} \frac{1}{b(z)} = \frac{1}{b_0} \{ & 1 - B_1^{(0)}z - \dots - B_3^{(0)}z^3 \} + \{ (B_1^{(0)})^2 z^2 \\ & + 2B_1^{(0)}B_2^{(0)}z^3 + \dots \} - [B_1^{(0)}]^3 z^3 - \dots, \end{aligned} \quad (C.3a)$$

and rearranging the above series into successive powers of z produces

$$\frac{1}{b(z)} = \frac{1}{b_0} + D_{b1}^{(0)}z + D_{b2}^{(0)}z^2 + D_{b3}^{(0)}z^3 \dots \quad (C.3b)$$

where

$$\begin{aligned} D_{b1}^{(0)} &= -B_1^{(0)}, D_{b2}^{(0)} = -B_2^{(0)} + [B_1^{(0)}]^2 \\ D_{b3}^{(0)} &= -B_3^{(0)} + 2B_1^{(0)}B_2^{(0)} - [B_1^{(0)}]^3. \end{aligned} \quad (C.4)$$

To obtain an expression for $\ln\{b(z)/a(z)\}$ consider the expression

$$\begin{aligned} \ln\left[\frac{b(z)}{a(z)}\right] &= \ln\frac{b_0}{a_0} + \ln\{1 + B_1^{(0)}z + \dots + B_3^{(0)}z^3\} \\ &\quad - \ln\{1 + A_1^{(0)}z + \dots + A_3^{(0)}z^3\} \end{aligned} \quad (C.5)$$

Taking the reciprocal of eq (C.5) and using the geometric expansion yields

$$\begin{aligned} \ln\left[\frac{b(z)}{a(z)}\right]^{-1} &= \left\{ \ln\frac{b_0}{a_0} \right\}^{-1} \left\{ 1 - \left[\ln\frac{b_0}{a_0} \right]^{-1} \left\{ \ln[1 + B_1^{(0)}z \right. \right. \\ &\quad \left. \left. + \dots \right] + \ln[1 + A_1^{(0)}z + \dots] \right\} \\ &\quad + \left\{ \ln\frac{b_0}{a_0} \right\}^{-2} \{ \ln^2(1 + B_1^{(0)}z + \dots) \\ &\quad - 2 \ln[1 + B_1^{(0)}z + \dots] \ln[1 + A_1^{(0)}z + \dots] \\ &\quad + \ln^2[1 + A_1^{(0)}z + \dots] \}. \end{aligned} \quad (C.6)$$

From the absolutely and uniformly convergent expansion

$$\ln\{1 + \omega\} = \omega - \frac{\omega^2}{2} + \frac{\omega^3}{3} + \dots$$

for $|\omega| \leq a_0 < 1$

the expansion eq (C.6) is rearranged in powers of z to obtain

$$\left\{ \ln\frac{b(z)}{a(z)} \right\}^{-1} = \sum_{n=0}^{\infty} H_n^{(1)} z^n \quad (C.7)$$

where the first four coefficients are defined as

$$\begin{aligned} H_0^{(1)} &= \left\{ \ln\frac{b_0}{a_0} \right\}^{-1} \\ H_1^{(1)} &= - \left\{ \ln\frac{b_0}{a_0} \right\}^{-2} \{ G_{b0}^{(1)} - G_{a0}^{(1)} \} \\ H_2^{(1)} &= - \left\{ \ln\frac{b_0}{a_0} \right\}^{-2} \{ G_{b1}^{(1)} - G_{a1}^{(1)} \} \\ &\quad + \left\{ \ln\frac{b_0}{a_0} \right\}^{-3} \{ G_{b0}^{(2)} - 2G_{b0}^{(1)}G_{a0}^{(1)} + G_{a0}^{(2)} \} \\ H_3^{(1)} &= - \left\{ \ln\frac{b_0}{a_0} \right\}^{-2} \{ G_{b2}^{(1)} - G_{a2}^{(1)} \} \\ &\quad + \left\{ \ln\frac{b_0}{a_0} \right\}^{-3} \cdot \{ G_{b1}^{(2)} - 2G_{b1}^{(1)}G_{a0}^{(1)} - 2G_{b0}^{(1)}G_{a1}^{(1)} + G_{a1}^{(2)} \} \\ &\quad - \left\{ \ln\frac{b_0}{a_0} \right\}^{-4} \{ G_{b0}^{(3)} - 3G_{b0}^{(2)}G_{a0}^{(1)} + 3G_{b0}^{(1)}G_{a0}^{(2)} + G_{a0}^{(3)} \} \end{aligned} \quad (C.8)$$

and the G coefficients for the outer conductor are

$$\begin{aligned} G_{b0}^{(k)} &= [B_1^{(0)}]^k; k = 1, 2, 3. \\ G_{b1}^{(1)} &= B_2^{(0)} - \frac{[B_1^{(0)}]^2}{2}, \\ G_{b1}^{(2)} &= 2G_{b0}^{(1)}G_{a1}^{(1)} = 2B_1^{(0)} \left\{ B_2^{(0)} - \frac{[B_1^{(0)}]^2}{2} \right\}, \\ G_{b2}^{(1)} &= B_3^{(0)} - B_1^{(0)}B_2^{(0)} + \frac{[B_1^{(0)}]^3}{3}. \end{aligned} \quad (C.9)$$

The G coefficients for the inner conductor are computed by replacing $B_k(0)$ with $A_k(0)$. To obtain the expansion for κ in eq (1.15) an expression for $K[\phi(z)]$ needs to be found. From eqs (3.1) and (1.1)

$$K[\phi_b(z)] = \frac{1 + \sin[\phi_b(z)]}{1 + \tan[\phi_b(z)]}, \quad (C.10)$$

$$K[\phi_b(z)] = \frac{1 + b'(z)/\{1 + b'(z)\}^2}{1 + b'(z)}.$$

Using the binomial and geometric expansions, in the last expression, yields the following expression in terms of spline coefficients

$$K[\phi_b(z)] = 1 - \frac{3}{2} b_1^2 - 6 b_1 b_2 z.$$

We now have from eqs (C.3), (C.7), and (C.10) the expression

$$\frac{K\{\phi_b(z)\}}{b(z) \ln \frac{b(z)}{a(z)}} = \left\{ 1 - \frac{3}{2} b_1^2 - 6 b_1 b_2 z \right\} \sum_0^3 D_n^{(0)} z^n \sum_0^3 H_m^{(1)} z^m = \sum_0^3 C_{bk}^{(1)} z^k \quad (C.11)$$

where $C_k^{(1)}$ is the convolution of coefficients, i.e.,

$$\begin{aligned} C_{b0}^{(1)} &= \left(1 - \frac{3}{2} b_1^2\right) D_0^{(0)} H_0^{(1)} \\ C_{b1}^{(1)} &= \left(1 - \frac{3}{2} b_1^2\right) \{D_0^{(0)} H_1^{(1)} + H_0^{(1)} D_1^{(0)}\} \\ &\quad - 6 b_1 b_2 D_0^{(0)} H_0^{(1)} \\ C_{b2}^{(1)} &= \left(1 - \frac{3}{2} b_1^2\right) \sum_{k=0}^2 D_{2-k}^{(0)} H_k^{(1)} - 6 b_1 b_2 \sum_{k=0}^1 D_{1-k}^{(0)} H_k^{(1)} \\ C_{b3}^{(1)} &= \left(1 - \frac{3}{2} b_1^2\right) \sum_{k=0}^2 D_{3-k}^{(0)} H_k^{(1)} - 6 b_1 b_2 \sum_{k=0}^1 D_{2-k}^{(0)} H_k^{(1)}. \end{aligned} \quad (C.12)$$

Since the inner conductor expansion proceeds in the same way, the total expression is

$$\kappa(z) = \sum_{k=0}^3 C_k^{(2)} z^k \quad (C.13)$$

where

$$C_k^{(2)} = C_{ak}^{(1)} + C_{bk}^{(1)}. \quad (C.14)$$

The transfer coefficient eq (2.4) has the expansion

$$\begin{aligned} T_{00}(z) &= [b_1 + 2b_2 z + 3b_3 z^2] \left[\sum_{k=0}^3 D_{bk}^{(0)} z^k \right] \left[\sum_{k=0}^3 H_{bk}^{(1)} z^k \right] \\ &\quad - [a_1 + 2a_2 z + 3a_3 z^2] \sum_{k=0}^3 D_{ak}^{(0)} z^k \sum_{k=0}^3 H_{ak}^{(1)} z^k, \\ T_{00}(z) &= \sum_{k=0}^3 C_k^{(3)} z^k. \end{aligned} \quad (C.16)$$

where

$$\begin{aligned} C_n^{(3)} &\equiv \sum_{m=\mu(n)}^n \sum_{k=0}^m \{(n \mp 1 = m) b_{n+1-m} D_{bm-k}^{(0)} H_k^{(1)} \\ &\quad - (n+1-m) a_{n+1-m} D_{am-k}^{(0)} H_k^{(1)}\} \end{aligned}$$

$$\begin{aligned} \text{and } \mu(n) &= 0 \text{ for } n < 3, \\ &= 1 \text{ for } n = 3. \end{aligned} \quad (C.17)$$

From eqs (2.3), (C.14), and (C.17) set

$$\delta_0^{(1)} = j\beta + \frac{Z_s}{2k_0} C_0^{(2)} \quad (C.18)$$

$$\delta_k^{(1)} = \frac{Z_s}{2k_0} C_k^{(2)}; k \geq 1 \quad (C.19)$$

$$\delta_k^{(2)} = \frac{Z_s}{2k_0} C_k^{(2)} + \frac{C_k^{(3)}}{2}; k \geq 0. \quad (C.20)$$

The coefficients $\nu_{k,m-1}^{(2)}$ in eq (3.14) are defined by selecting the coefficients of η^k and convoluting the series product. Let

$$\begin{aligned} \nu_{0,m-1}^{(1)} &= 1 \\ \nu_{1,m-1}^{(1)} &= 0 \\ \nu_{2,m-1}^{(1)} &= -\delta_{1,m-1}^{(1)} \\ \nu_{3,m-1}^{(1)} &= -\frac{2}{3} \delta_{2,m-1}^{(1)} \\ \nu_{4,m-1}^{(1)} &= -\frac{1}{2} \delta_{3,m-1}^{(1)} + \frac{1}{2} \{\delta_{1,m-1}^{(1)}\}^2 \\ \nu_{5,m-1}^{(1)} &= \frac{2}{3} \delta_{1,m-1}^{(1)} \delta_{2,m-1}^{(1)} \\ \nu_{6,m-1}^{(1)} &= 2 \left\{ \frac{\{\delta_{2,m-1}^{(1)}\}}{3^2} + \frac{1}{4} \delta_{1,m-1}^{(1)} \delta_{3,m-1}^{(1)} \right\} \\ \nu_{7,m-1}^{(1)} &= \frac{1}{3} \delta_{2,m-1}^{(1)} \delta_{3,m-1}^{(1)} \\ \nu_{8,m-1}^{(1)} &= \frac{1}{8} \left\{ \delta_{3,m-1}^{(1)} \right\}^2 - \frac{1}{6} \left\{ \delta_{1,m-1}^{(1)} \right\}^3 \end{aligned} \quad (C.21)$$

Proceeding to $\nu_{k,m-1}^{(2)}$

$$\nu_{k,m-1}^{(2)} = \sum_{\ell=0}^{\mu_1(k)} \delta_{k-\ell,m-1}^{(2)} \nu_{\ell,m-1}^{(1)} \quad (C.22)$$

where

$$\begin{aligned} \mu_1(k) &= k \text{ if } 0 \leq k \leq 3 \\ &= 3 \text{ if } 3 < k \leq 8 \end{aligned} \quad (C.23)$$

and

$$\nu_{k,m-1}^{(2)} = \sum_{\ell=k-8}^3 \delta_{k-\ell,m-1}^{(2)} \nu_{\ell,m-1}^{(1)} \text{ if } 8 < k \leq 11. \quad (C.24)$$

Appendix D

Expression of the contour length ℓ_0 in terms of the spline coefficients is initiated from the definition

$$\ell_0 = \int_0^{2\pi} \left\{ \zeta(\theta) + \zeta^{-2}(\theta) \left[\frac{\partial \zeta}{\partial \theta} \right]^2 - \dots \right\} d\theta. \quad (D.1)$$

Using the spline coefficients for the interval $[\theta_n, \theta_{n+1}]$ yields the representation

$$P_n(\eta) = \sum_{k=0}^3 P_{1,k,n}^{(1)} \eta^k, \quad 0 \leq \eta \leq \theta_{n+1} \quad (D.2)$$

at $n=0$, $P_n(0) = P_{1,0,n}^{(1)}$ = the measurement of ζ at $\theta = \theta_n$. Then eq (D.1), in view of eq (D.2), yields

$$\begin{aligned} \ell_0 = & \sum_{n=0}^{N-1} \int_0^{\theta_{n+1}-\theta_n} \left\{ \sum_{k=0}^3 P_{1,k,n}^{(1)} \theta^k \right. \\ & \left. + \frac{1}{2} \left[\sum_{k=0}^3 (k+1) P_{1,k+1,n}^{(1)} \theta^k \right]^2 \frac{1}{\sum_{k=0}^3 P_{1,k,n}^{(1)} \theta^k} \right\} d\theta. \end{aligned} \quad (D.3)$$

The denominator can be expanded into a geometric series such that the second term above yields

$$\begin{aligned} \sum_{k=0}^7 P_{2,k,n}^{(1)} \theta^k = & \left\{ \sum_{k=0}^3 (k+1) P_{1,k+1,n}^{(1)} \theta^k \right\}^2 \left\{ \frac{1}{P_{1,0,n}^{(1)}} \right\} \\ & \cdot \left\{ 1 - \frac{P_{1,1,n}^{(1)}}{P_{1,0,n}^{(1)}} \theta - \dots - \frac{P_{1,3,n}^{(1)}}{P_{1,0,n}^{(1)}} \theta^3 + \dots \right\} \end{aligned} \quad (D.4)$$

and eq (D.3) on substituting eq (D.4) yields the form eq (4.13). For other values of p and q we have

$$\begin{aligned} h_{pq} = & \frac{1}{\ell_0} \sum_{n=0}^{N-1} e^{j(p-q)\theta_n} \int_0^{\theta_{n+1}-\theta_n} \left\{ \sum_{k=0}^{3(p+q+1)} P_{1,k,n}^{(p+q+1)} \theta^k \right. \\ & \left. + 1/2 \left[\sum_{k=0}^{3(p+q+1)} P_{1,k,n}^{(p+q-1)} \theta^k \right] \left[\sum_{k=0}^2 (k+1) P_{1,k+1,n}^{(1)} \theta^k \right]^2 \right\} \\ & \cdot e^{j(p-q)\theta} d\theta \end{aligned} \quad (D.5)$$

where

$$\sum_{k=0}^{3(p+q)} P_{1,k,n}^{(p+q)} \theta^k = \left\{ \sum_{k=0}^3 P_{1,k,n}^{(1)} \theta^k \right\}^{p+q}. \quad (D.6)$$

Let $P_{2,k,n}^{(p+q-1)}$ be the convolution of the product $P_{2,k,n}^{(p+q-1)}$ and $\{(k+1) P_{1,k+1,n}^{(1)}\}^2$ above. Then eq (D.5) yields

$$\begin{aligned} h_{pq} = & \frac{1}{\ell_0} \sum_{n=0}^{N-1} e^{j(p-q)\theta_n} \sum_{k=0}^{3(p+q+1)} P_{1,k,n}^{(p+q+1)} \{S_k[(\theta_{n+1}-\theta_n) \\ & \cdot (p-q)j] - S_k(0)\} + \frac{1}{2} \sum_{k=0}^{3(p+q+1)} \{e^{j(p-q)\theta_n}\} P_{2,k,n}^{(p+q+1)} \\ & \cdot \{S_k[(\theta_{n+1}-\theta_n)(p-q)j] - S_k(0)\} \end{aligned} \quad (D.7)$$

where S_k is defined in eq (3.11).

Conference Reports

FOURTH INTERNATIONAL SYMPOSIUM ON RESONANCE IONIZATION SPECTROSCOPY AND ITS APPLICATIONS *National Bureau of Standards, Gaithersburg, MD, April 10–15, 1988*

The technique of resonance ionization spectroscopy (RIS), makes use of the resonant absorption of photons via allowed electronic transitions to transfer an electron in a neutral gaseous atom (or molecule) from some initial state through various excited states to the continuum. This process can be elementally, even isotopically, selective. The product is an ion pair, and either the electron or the cation of the pair can be detected.

The present symposium is the latest in a biannual series of meetings dealing with the photophysics of the RIS process in its many forms, with proposed applications and with descriptions of developed applications. It is quite apparent that, over the course of these four symposia, emphasis of the meetings has shifted from the fundamentals and proposed experiments to actual applications. A considerable effort is also now underway on molecular RIS. This aspect of the field has seen a significant growth

from the last meeting as evidenced by the increase in the number of papers on this topic.

A number of interesting and timely papers were presented, but only a few selected highlights can be described here. That RIS techniques are presently in use for acquiring real analytical results was evident in the work presented by R. Willis and coworkers at Atom Sciences, Inc. (Oakridge, TN) dealing with the determination of very low amounts of ^{81}Kr in ground water samples. These analyses are used to determine the age of such water samples. Modern water contains 1000 atoms of ^{81}Kr per liter. From 50-liter samples of water obtained from a location in Canada, about 6000 atoms of ^{81}Kr were found. From a comparison of this number to the ^{81}Kr found in an equivalent modern air samples, the age of the ground water can be deduced. The sensitivity of this RIS determination of ^{81}Kr is well beyond the sensitivity of the established radioactive counting techniques.

In an experiment designed to measure the fundamental structure of simple atoms and molecules, S. R. Lundeen of the University of Notre Dame detected weakly populated Rydberg states of He and H_2 by RIS techniques. RIS is the method of choice and really the only technique that can easily produce the information required in this study.

Several papers addressed the ability of RIS to detect and determine transient and/or short-lived species. A particular example of this application involved the study by U. Kronert and coworkers (from the University of Mainz, West Germany) of short-lived ^{185}Au and ^{184}Au isotopes (half-lives of 4.3 min and 53 s, respectively), generated and implanted in graphite. About 60% of some 5×10^9 atoms were laser desorbed from the foil and then resonantly ionized and mass analyzed by a three-color RIS process. As one result of this experiment, hyperfine splitting and isotope shift information was obtained for the isotope investigated.

A paper by G. Bekov, from the U.S.S.R. Academy of Sciences, was of particular interest. He presented a description of their laser process that involves optical excitation followed by electric field ionization. Their studies have been applied to ultrasensitive detection of elements of geochemical interest. Their results support the theory of Alvarez for an extraterrestrial origin of the Cretaceous-Tertiary boundary.

The RIS technique has now been sufficiently studied so that realistic assessment of the current limitations can be made. Papers and posters dealing with this aspect were presented. Two points might be emphasized here. The sample matrix does influence the magnitude and composition of the evolved species that are required for RIS study. This point was brought out in the third symposium and became more apparent in this meeting. Matrix effects do not destroy the usefulness of the technique, but they do need to be addressed in analytical applications. A second problem, that is becoming more obvious as the precision of the technique improves, is that of bias in isotope ratio measurements carried out by resonance ionization mass spectrometry (RIMS). These bias effects appeared in results of several studies and were discussed formally and informally during the meeting. It seems obvious that further evaluation of these effects will be made, and the results will appear in the literature and be presented in the fifth symposium scheduled to be held in Ispra, Italy, in 1990.

The symposium was truly international. Over 150 participants attended from nearly 20 countries, including the U.S.S.R. for the first time. It was funded by a number of organizations: Office of Health and Environmental Research of the U.S. Department of Energy, U.S. Air Force Office of Scientific Research, Battelle Pacific-Northwest Laboratories, EG&G Corporation, Department of Commerce, National Bureau of Standards, National Science Foundation, and the University of Tennessee. The detailed proceedings has been published by the Institute of Physics, Techno House, Bristol, U.K., under the title "Resonance Ionization Spectroscopy 1988," Conference Series No. 94.

J. P. Young
Analytical Chemistry Division
Oak Ridge National Laboratory
Oak Ridge, TN 37831

News Briefs

Developments

CONDUCTIVITY MEASUREMENTS ON INSULATING FOAMS

Polymethacrylimide (PMA) and polyurethane foams are used as thermal insulation in many applications, including the vacuum of high altitudes and outer space. In work done for NASA's Langley Research Center, NIST measured the thermal conductivity of several foams in a guarded-hot-plate apparatus at temperatures of about 100 to 300 kelvin (-280 to 80 °F). Most of the tests were done in dry nitrogen gas at slightly above ambient pressure, with one test repeated at 0.67 Pa (six millionths of an atmosphere). The specimens included neat PMA foams, a PMA foam sandwiched between layers of glass cloth, adhesive, and aluminized polyimide film, and polyurethane foam sprayed onto a 2-mm-thick aluminum substrate. The apparent conductivity of the vacuum-tested sample (polyurethane-aluminum) was lower than the same sample tested in gas, probably because the vacuum reduced the heat transfer between the sample and the apparatus' hot plate. Results of these tests are presented in Thermal Conductivity of Selected Foams and Systems from 100 to 300 K (NBSIR 88-3086), available from the National Technical Information Service, Springfield, VA 22161, for \$14.95 prepaid. Order by PB #88-201553.

DEVELOPMENT OF STANDARD WELD PROCEDURES

Ten Welding Procedure Specifications (WPS) were developed for steel plate and sheet in a cooperative program with industry and are being submitted to the American National Standards

Institute (ANSI) for approval as ANSI standards. The WPSs were validated based on hundreds of NIST test results.

Determination of acceptable mechanical properties in these welds defines the range of parameters allowed in an approved WPS. Until now, each welding firm has been required to develop its own WPSs for each materials, electrode, and set of welding parameters that they plan to use. Publication of approved WPSs will allow these firms to be more productive by transferring their efforts to other activities such as product quality control.

The first two WPSs were for steel plates near 10-mm in thickness. The specimen preparation, testing, and review was performed by a team with members from the Welding Research Council Welding Procedures Committee, NIST, independent testing firms, and industry inspection agencies. The eight WPSs for sheet metal (10 and 18 gauge) were produced by this same team with special assistance from the National Training Fund (a union-fabricator organization dedicated to supporting the sheet metal industry). After review by the WRC committee, they have been submitted to the American Welding Society before being forwarded to ANSI. Further WPS development is being directed toward other materials and welding processes.

CHARACTERIZATION OF ASPHALTIC CEMENTS

The Strategic Highway Research Program (SHRP) is funding a joint Montana State University (MSU)-NIST project aimed at explaining the complex chemical structure of asphaltic cements used in highway pavements. The project brings together expertise in asphalt chemistry at MSU and in solid-state nuclear magnetic resonance (NMR) measurements of complex materials at NIST. SHRP is a federal program aimed at providing

research which will lead to improved materials and practices for the nation's highways and bridges.

The MSU-NIST project is based on the hypothesis that molecules in asphaltic cements are diverse in structure and in time will segregate according to similarities of structure. This process will result in molecular aggregation which will be followed as a function of time and temperature in the NMR experiments. Understanding the time and temperature behavior of molecular aggregation should lead to new insights into relationships among chemical structure, aging of pavements, mechanical performance, and optimal service temperatures. The NMR studies will be coordinated with research into mechanical properties and performance of asphalts conducted by other SHRP contractors. Improved specifications for asphalts are the anticipated output of the combined effort.

STRUCTURE MODULATED CHROMIUM ENHANCES WEAR PERFORMANCE

Recent developments in the electrodeposition group on modulating the crystallographic orientation of grains in chromium are expected to lead to significant advances in wear performance for many applications. By controlling some of the deposition parameters such as electrolyte temperature, current density, and pulse duty cycle, the crystallographic orientation can be controlled. Microlayered chromium has been found to have an apparent anisotropic deformation which depends on layer spacing. This anisotropy is insignificant at spacing of 1 to 3 nanometers, but becomes significant at spacings of about 400 angstroms. Microhardness of microlayered chromium was found to be very high within the range of 1500-1800 Knoop hardness (KHN/25 g) at spacings of 10 to 30 angstroms. At loads above 25 g cracking was observed.

DISCOVERY OF PERVASIVE ANTIPHASE BOUNDARIES IN LIQUID ENCAPSULATED CZOCHRALSKI-GROWN SEMI-INSULATING UNDOPED GALLIUM ARSENIDE

Novel, pervasive streak-like features restricted to the direction of the scattering vector have been observed in diffraction images of monochromatic synchrotron radiation transmitted through liquid encapsulated Czochralski (LEC)-grown semi-insulating gallium arsenide. The appearance of such features is not predicted by commonly accepted dynamical diffraction imaging theory, but can be interpreted by dynamical theory that has been generalized to include scattering by imperfect crystals.

As a result, these observations have been shown to be caused by the disruption of diffraction by very thin {110} boundaries characterized by lattice coherence but incorporating a phase shift. Of the various possible crystal defects, only antiphase boundaries are consistent with these observations as well as with the other aspects of the new high-resolution diffraction images: (quasi)cellular structure, linear, very low-angle subgrain boundaries in $\langle 110 \rangle$ directions, surface stripes in a $\langle 110 \rangle$ direction, and systematic differences in the acceptance angle for images involving various diffraction vectors. Some of the individual features had been observed at lower resolution, indicating that the crystals in the NIST study are typical of LEC material. However a unified interpretation had not been achieved. The observation of pervasive antiphase regions suggests that approaches to greater crystal perfection, which is required for the commercial exploitation of gallium arsenide for high-speed information processing, must be fundamentally reconsidered. The new observations have been carried out on the NIST materials science beam lines at the National Synchrotron Light Source, which provides diffraction imaging resolution not elsewhere available, and were developed with special DOC funding.

INTERCOMPARISON OF RADIOMETRIC STANDARDS IN THE NEAR INFRARED

The Radiometric Physics Division of the Center for Radiation Research (in Gaithersburg) and the Electromagnetic Technology Division (in Boulder) of the Center for Electronics and Electrical Engineering have carried out an intercomparison to demonstrate the level of agreement of near infrared power measurements between the two divisions. The intercomparison will ultimately improve the accuracy of laser power measurements by the fiber optics communications industry. The transfer standards were two electrically calibrated pyroelectric radiometers (ECPRs), which were calibrated at 1.32 micrometers and power levels of 0.1 and 1.0 mW using different measurement procedures and instrumentation.

At Boulder, the NIST C-series calorimeter system with a calibrated wedge beamsplitter served as the absolute standard. At Gaithersburg, the absolute measurements were based on the predictable quantum efficiency (self-calibration) of silicon photodiodes in the visible part of the spectrum. The auxiliary instrument used to extend the absolute measurements to radiant power measurements at 1.32 micrometers was a cavity type electrically

calibrated radiometer. If the overall agreement between the two laboratories is expressed as the ratio of the Gaithersburg values to the Boulder values, the ratio is 1.0047 with a combined estimated uncertainty (three sigma) of ± 0.61 percent. A portion of the disagreement between the two laboratories results from the manner in which the ECPR transfer standards were used. The staff from the two divisions plan further intercomparisons, which are expected to yield improved results.

NEW CALCULATIONS OF INELASTIC MEAN FREE PATHS FOR LOW-ENERGY ELECTRONS IN SOLIDS

The inelastic mean free path (IMFP) of low-energy (50-2000 eV) electrons in solids is a vital parameter in surface science since it determines the sensitivity of many of the spectroscopic techniques involving electron beams. In addition, the IMFP is important because it is required for quantitative surface analysis by Auger-electron spectroscopy and x-ray photoelectron spectroscopy, two techniques in widespread use. Unfortunately, it has proven difficult to calculate or measure IMFPs with the needed accuracy.

Recently, David R. Penn of the Radiation Physics Division developed a new hybrid algorithm for computing IMFPs. Experimental optical data are used to represent the dependence of the inelastic scattering probability on energy loss, and the theoretical Lindhard dielectric function is used to represent the scattering probability on momentum transfer. Optical data for various materials are used because the data can be checked for internal consistency by various sum rules and because it is not necessary to make assumptions about the various modes of inelastic scattering and their relative strengths.

The Penn algorithm has been applied to IMFP calculations of 200-2000 eV electrons in 31 materials by S. Tanuma (a guest scientist from Nippon Mining Company) and Cedric J. Powell (Surface Science Division). The calculations were made for 27 elements and four compounds that had the needed optical data. The computed IMFPs for each material were fitted to the Bethe equation for inelastic electron scattering in matter. From these fits, a general IMFP equation was empirically derived from which IMFPs could be predicted in terms of several material parameters. The new IMFP formula will be particularly useful for predicting the IMFP dependence on electron energy for a given material and the material-dependence for a given energy.

Penn has developed a more complex algorithm that can be used to calculate IMFPs with electron energies down to about 50 eV. These calculations are in progress.

OPTICAL PROBES DEVELOPED FOR ELECTROMAGNETIC FIELD MEASUREMENTS

To meet needs for measuring time-varying electromagnetic fields with improved accuracy and with various environmental constraints, CEE's Electromagnetic Fields Division has developed electric field probes based on electro-optical modulators and fiber optic data links.

These systems provide amplitude and phase information for high-frequency (gigahertz-range) fields; cause minimum distortion of the field; are immune from electromagnetic pickup and interference in the leads; and can be deployed in areas where an electrical discharge might be hazardous. The first operational electro-optic field sensor to be developed at NIST incorporates resistively-tapered dipole antenna elements and a bulk-crystal lithium niobate modulator. The upper frequency limit for this probe is about 1 GHz. Another type uses an integrated optic modulator of a modified directional coupler design to cover frequencies between 10 kHz and 4 GHz. This modulator is biased to an operating wavelength (typically 840 nm) chosen to provide the maximum linear dynamic frequency response.

TOO HOT TO HANDLE, BUT NOT TO MEASURE

Trying to measure the melting point of graphite at atmospheric pressure is a lesson in disappearing acts. The graphite evaporates. A NIST researcher has developed a technique to avoid that problem with a measuring system that allows investigation of materials properties at temperatures ranging from 1300 to 6000 K. Even 10,000 K is within reach of the system. Practical applications include space-related work, where temperatures soar during reentry, nuclear reactor safety, and defense, specifically rocketry. The secret to the system, which took 10 years to design, develop, construct, and make operational, is extremely rapid measurements, taken in microseconds (millionths of a second). The rationale is that if you conduct the experiment in a very, very short time, many measurement problems associated with hostile environments, while still present, are minimized.

NIST/IBM NEUTRON REFLECTION STUDIES OF POLYMER SURFACES AND INTERFACES

Scientists from the Reactor Radiation Division and from IBM Almaden Research Center induced ordering of diblock copolymers. Block copolymers are increasingly being used in applications such as protective coatings, adhesives, and surfactants which specifically exploit their surface properties.

The diblock copolymers in this study are polystyrene/polymethylmethacrylate (PS/PMMA) where either PS or PMMA block was perdeuterated to increase the contrast between two blocks. Neutron reflectivity measurements from their films (1000-2000 Å) of these block copolymers show the phase separation of the block copolymers into a lamellar morphology with a remarkable degree of orientation of the lamellae parallel to the surface. With this technique we have determined the detailed shape of the profile of the interface between PS and PMMA blocks and the repeat distance of the PA and PMMA blocks in the lamellae.

Currently experiments are being extended to study the effects of molecular weight, deuteration, various different substrates (e.g., quartz, silicon, sapphire) and temperature on interfacial profiles of the lamellae.

This research represents just one of the many potential applications of neutron reflection techniques for the study of near surface and interfacial structures in materials, thin films, and liquids.

DIAMOND FILMS EXAMINED

Cathodoluminescence imaging and spectroscopy experiments have been conducted in a scanning electron microscope to obtain information regarding the presence and distribution of impurities and defects in diamond films prepared by the hot filament chemical vapor deposition method. Diamond is a potential high-performance transistor, optical emitter, and ultraviolet detector material whose performance will be affected by the presence of such defects and impurities. By comparing the cathodoluminescence spectra in our diamond films to spectra reported in the literature for bulk diamonds, we have tentatively identified defects associated with nitrogen impurity atoms, interstitials, atomic vacancies, and dislocation lines.

Cathodoluminescence imaging indicates that these defects are not homogeneously distributed throughout the material; four-fold symmetric crystal faces luminesce strongly but three-fold crystal faces show almost no cathodoluminescence. The presence of the defects was found to depend on the

deposition temperature. Work is under way to examine how other processing variables affect the presence of the defects.

SUCCESSFUL VALIDATION BY THE KEY MANAGEMENT VALIDATION SYSTEM

The Key Management Validation System (KMVS) developed by National Computer Systems Laboratory (NCSL) has been used to validate a device for conformance to an industry standard for Financial Institution Key Management (Wholesale), ANSI X9.17. This standard gives rules and protocols for manual and automatic key distribution used for encryption and message authentication in point-to-point and key center environments. Developed under Treasury Department sponsorship over a 2-year period, the KMVS tests the electronic distribution of keys in a point-to-point environment; the device was validated using a restricted set of options appropriate for federal government use.

In the final testing of the validation software, NCSL worked with Codercard, Inc., which developed the device. Testing was accomplished through ordinary telephone lines between the Codercard facility in California and the KMVS at NCSL. An earlier remote validation system, the Message Authentication Code Validation System, has been used to validate 16 devices for conformance to FIPS 113, Computer Data Authentication.

NEW PROBE CHARACTERIZATION TECHNIQUE PROMOTES MORE EFFICIENT USE OF GEOSTATIONARY ORBIT FREQUENCY SPACE BY COMMUNICATIONS SATELLITES

Staff of CEEE's Electromagnetic Fields Division have developed new analyses and associated techniques for characterizing the dual-port, circularly polarized probes used by the division and others in carrying out near-field antenna scanning measurements of communications satellite antennas. The division characterizes probes used by virtually all U.S. near-field ranges. The new techniques provide reduced uncertainty in the quantities probe axial ratio (from 0.05 to 0.02 dB) and tilt angle (from 30 to 5 degrees), which provide a measure of polarization isolation. The degree of polarization isolation achieved affects the channel capacity of satellites broadcasting signals at the same frequency, but with differing polarizations. Both physical orbital space and frequency space within the designated bands are scarce commodities, with pressures being

applied from lesser-developed countries on the developed nations to move to higher-frequency bands for which the technology is still evolving.

The new NIST techniques have the additional advantage that they are more efficient because they do not require a separate set-up: the measurements are made between three probes taken in pairs in rotation with the same apparatus used for gain and pattern measurements. All three probes can be unknowns at the beginning of the measurements. The reduced uncertainty is a result of an improved theory and a measurement technique that uses both amplitude and phase information, in which the measurements are made over large dynamic range rather than for very small variations in signal level.

VOLT, OHM STANDARDS TO CHANGE INTERNATIONALLY IN 1990

National representatives of the world's weights and measures community met recently in Sèvres, France, to adopt new conventional values for the Josephson constant and the von Klitzing constant. These are the fundamental physical constants required to determine operational values of the volt, using the Josephson effect, and the ohm, using the quantum Hall effect. The changes, approved by the International Committee of Weights and Measures (CIPM), will take effect January 1, 1990. All industrial nations will share, for the first time, a common practical basis for measuring voltage and resistance. Prior to this, there was a difference of approximately 1.2 ppm (parts-per-million) between the U.S. voltage standard and that of most European countries purely because of differences in the way the national standards were maintained. With the advent of modern, high-precision voltmeters, such differences have become increasingly significant to U.S. firms seeking to export high-precision equipment. For the U.S., the new values mean that NIST will adjust the U.S. voltage standard by about 9.3 ppm, and the U.S. resistance standard by about 1.7 ppm. Precision electrical measuring instruments will have to be adjusted or recalibrated to maintain consistency with the new national standards. (See detailed article in this issue.)

TEST INSTRUMENT TO DETECT COMPUTER FLAWS PATENTED

A test instrument designed by researchers from NIST and private industry to verify the correctness of information exchanges between large electronic devices recently was granted a patent

(no. 4,764,863). It offers the designers, builders, and users of complex computer systems a powerful tool for tracking down subtle flaws in equipment in a way previously not possible. Most flaw-detecting instruments are programmed to "trigger" only when certain, predetermined events happen. This instrument can be programmed with an idealized model of a properly operating system; it then monitors the system until something out of the ordinary is encountered. At that point, recording circuits are triggered to memorize the anomaly. [Inventors are Robert B. J. Warnar, George G. Nacht, Philip Gaudette, and Arthur W. Holt (retired) of NIST and Lee J. Silverthorn of Software Resources, Inc., Paradise Valley, Ariz.] For licensing information, contact Office of Federal Patent Licensing, National Technical Information Service, Springfield, VA 22161; telephone: 703/487-4732.

BETTER SHEET METAL PRODUCTS WITH LESS WASTE

Manufacturers of goods fabricated from sheet metal may be able to cut down on waste and scrap thanks to an ultrasonic test developed by NIST working with universities and industry groups. Project collaborators are NIST, Iowa State University, Colorado School of Mines, and the Advanced Steel Processing and Products Research Center at the Colorado School of Mines. A major concern of manufacturers of cars, trucks, appliances, metal furniture, cans, and other items formed or stamped from steel and aluminum sheet is the problem of insufficient or variable formability. The new NIST method uses an electromagnetic-acoustic transducer (EMAT) to launch ultrasonic waves into the sheet metal to measure texture and formability. Ultrasonic measurements have shown a high degree of correlation with traditional measures of formability in the specimens of thin steel examined so far, and the tests have covered the range of formability characteristics typically found in industrial applications.

MAKING INVENTION PAY

For the past 9 years, the Energy-Related Inventions Program, sponsored jointly by NIST and the U.S. Department of Energy, has been bringing together inventors through a series of National Innovation Workshops. The workshops provide practical guidance and information to inventors, entrepreneurs, and innovative businesses. The remaining 1989 workshops are scheduled as follows: April 21-22, Norman, OK; June 2-3, Columbia, SC; Sept. 29-30, Ames, IA; and Oct. (date undecided),

Fairfax, VA. The fee is approximately \$80. Topics covered include patenting and protection, estimating the worth of an invention, licensing, marketing, new business start-up, financing, and the DoE/NIST Energy-Related Inventions Program. For further information, contact Office of Energy-Related Inventions, NIST, 209 Engineering Mechanics Bldg., Gaithersburg, MD 20899; telephone: 301/975-5500.

1989 NATIONAL QUALITY AWARD APPLICATIONS ISSUED

Applications for the 1989 Malcolm Baldrige National Quality Awards are now available. The 31-page application guidelines include a description of the award, an application form, detailed instructions for filling out the form, and specifics on the scoring criteria and examination. The guidelines are available at no cost by writing to the Malcolm Baldrige National Quality Award, NIST, A1123 Administration Bldg., Gaithersburg, MD 20899. The National Quality Award was established by law in 1987. Its purpose is to promote quality awareness, recognize quality achievements of U.S. companies, and publicize successful quality strategies. The deadline for applications is May 5, 1989.

SHEDDING NEW LIGHT ON WAYS TO CUT ENERGY DOLLARS

Carefully controlling air flow around lights, increasing mass in floors, and adding carpeting are some basic design features for more energy efficient buildings that could result in savings worth millions of dollars a year, say NIST researchers. Using a specially designed, computer controlled test room, the researchers are finding ways to help cut the billions spent annually to light and cool commercial buildings. The data from these tests will be used to develop design and engineering handbooks and to validate a detailed computer model of the test room. The model will allow designers to simulate other room arrangements and lighting and heating and ventilating systems to extend the range of the NIST findings.

TEST CAN HELP ENSURE INDUSTRIAL CHEMICAL PURITY

In numerous high-technology industrial processes, chemicals called reagents are used as integral parts of the processes. It is crucial that these chemicals be extremely pure. The electronics industry, for example, uses reagents in the manufacture of semiconductor devices and needs to ensure that these chemicals do not contaminate devices with impuri-

ties. Even trace impurity amounts—parts per million or lower—must be measured and controlled. To address this need, researchers in the NIST Center for Analytical Chemistry have created a technique using inductively coupled plasma/mass spectrometry (ICP-MS), which allows improved purity tests of reagents to be made. Analysis of high-purity reagents for contaminants is particularly demanding, requiring rigorous control over the laboratory environment and procedures. The ICP-MS instrument is well-suited to these demands and offers advantages such as high sensitivity (parts per billion or lower), broad coverage of elements, and ease in sample introduction. So far, NIST researchers have used ICP-MS to analyze hydrochloric, nitric, hydrofluoric, sulfuric, and perchloric acids, as well as high-purity water, with a 10-fold or more increase in sensitivity over other methods.

NEW CALIBRATION SERVICES OFFERED

The explosive growth of optical fiber use in the communications industry has resulted in a demand for calibration services. NIST's Boulder, Colo., laboratory now offers measurements of optical laser power and energy at wavelengths and power levels of interest to fiber optic producers and users. Measurements are based on a standard reference instrument called the C-series calorimeter. An electrically calibrated pyroelectric radiometer (ECPR) is calibrated against the calorimeter and is then used to calibrate optical power meters at wavelengths of 850, 1300, and 1550 nanometers. To improve calibration capabilities, NIST is preparing test measurement systems for detector linearity, detector uniformity, and detector spectral responsivity. These systems should be available in 6 months. For a paper outlining NIST's optical power measurement capabilities, contact Fred McGehan, Div. 360, NIST, 325 Broadway, Boulder, Colo. 80303. For more information on calibration services, contact Thomas R. Scott, Div. 724 same address, or phone 303/497-3651.

PAPERS AVAILABLE ON OPTICAL FIBER MEASUREMENTS

Researchers interested in advances in optical fiber measurement may obtain a copy of Technical Digest, Symposium on Optical Fiber Measurements, 1988. The 202-page NIST publication contains the summaries of all 42 papers presented at the fifth biennial Symposium on Optical Fiber Measurements, held at NIST's Boulder, CO, laboratories, September 20 and 21, 1988. Of particular interest are papers on optical time domain reflectometry,

the measurement of cut-off wavelength, and the characterization of planar optical waveguides. The volume, NBS (now NIST) Special Publication 748, is available for \$10 prepaid from the Superintendent of Documents, U.S. Government Printing Office, Washington, D.C. 20402. Order by stock no. 003-003-02878-9.

CHARACTERIZING TEM CELLS

NIST has pioneered in the use of transverse electromagnetic (TEM) cells for the generation of standard electromagnetic (EM) fields. Electronic equipment and/or components are inserted into TEM cells and tested for susceptibility to or emission of EM radiation. The cells are also used to calibrate portable probes for the measurement of EM fields. A new publication, *Generation of Standard Electromagnetic Fields in a TEM Cell* (TN 1319), documents the facilities and procedures used by NIST to generate these EM fields. In addition to advantages, limitations, and characteristics of TEM cells, the publication discusses setup and measurement procedures for users, uncertainties in the standard field, and statistical control of the system. Twelve references are reproduced to provide the details of material summarized in the text. Copies of the publication are available from the Superintendent of Documents, U.S. Government Printing Office, Washington, D.C. 20402. Order by stock no. 003-003-02898-3 for \$12 prepaid.

Standard Reference Data

CRYSTDAT: AN ONLINE RESEARCH AND ANALYTICAL TOOL

The CAN/SND Scientific Numeric Database Service of the Canada Institute for Scientific and Technical Information and the NIST Crystal Data Center (United States) have collaborated to make chemical, physical, and crystallographic data in NBS CRYSTAL DATA available through CRYSTDAT. CRYSTDAT is an online, state-of-the-art database search system that can be used by scientists worldwide. Within CRYSTDAT, specially designed scientific, database management, and computer systems software have been integrated to form a unified search and analysis system. Highly selective searches on a variety of chemical and physical parameters on 140,000 crystalline compounds of all classes can be carried out using Boolean logic. The scientific software is a product

of a continued research effort whose objective is to provide the user with the latest research and search tools.

CRYSTDAT is easily accessible worldwide. In general, only a local call to the nearest telecommunications network is required to access the system. Scientists in many disciplines can routinely use this powerful research and analytical tool. Recently, the system has been extensively used in research on materials design (e.g., high T_c superconductors, lasers, optical materials) and in phase characterization. For information on using CRYSTDAT contact: Manager CAN/SND, Canada Institute for Scientific and Technical Information, National Research Council Canada, Ottawa, Canada K1A 0S2. Scientific questions on the system can be addressed to John R. Rodgers of NRCC (1-613-993-3294) or Alan D. Mighell of NIST (1-301-975-6255).

MAJOR EXPANSIONS ANNOUNCED FOR MASS SPECTRAL DATABASE

More than 6,000 new analytical mass spectra have been added to the NIST/EPA/MSDC Mass Spectral Database, a major international resource for analytical chemists and for environmentalists to use in identifying unknown substances. The database now contains approximately 50,000 chemical compounds, and for the first time includes information on the structures of more than 40,000 of these compounds.

The NIST/EPA/MSDC Mass Spectral Database is available for personal computers (PCs) or lease in a magnetic-tape format for scientific instruments from the National Institute of Standards and Technology (NIST).

Major improvements to the PC version of the database include new software options for faster searches by a wide variety of approaches such as using any available spectral information, a special feature that permits users to develop a personal analytical mass spectra data file, and new computer graphics that show the molecular structures of approximately 40,000 chemical compounds.

The magnetic-tape format, which now contains both mass spectral and structural data, is primarily for the databases and search systems used in mass spectrometry instruments. The PC version is designed to provide the bench scientist with fast, easy access to large numbers of analytical mass spectra.

The PC version of the database was first issued in 1987 from the NBS/EPA/MSDC Mass Spectral Database that is in use worldwide in a computer-magnetic tape format and as a six-volume,

7,000-page reference. The collection of evaluated electron ionization mass spectra on organic and inorganic substances was put together originally by scientists at the Environmental Protection Agency (EPA) and the National Institutes of Health. EPA and the Mass Spectrometry Data Centre (MSDC) in Nottingham, England, collaborate with certain data evaluations.

Mass spectrometry is an analytical technique that is used widely in pharmaceutical, biological, and environmental research, as well as in the chemical industry. EPA requires the use of the NIST/EPA/MSDC database by environmentalists to identify pollutants.

The NIST Mass Spectrometry Data Center, established Oct. 1, 1988, is one of 24 data centers that make up the National Standard Reference Data System (NSRDS). Since 1963, the NIST Office of Standard Reference Data has been responsible for coordinating on a national basis the evaluation of numerical data in the physical sciences. The evaluation of chemical and physical properties of substances is carried out in the NSRDS network of data centers.

The new PC Version 2.0 of the NIST/EPA/MSDC Mass Spectral Database is available for \$975. It is designed to be stored on a hard disk of any AT-class or PS/2 PC, where it occupies between 9 and 22 megabytes, depending on how many search options are needed by the user. Users of the first personal computer database, PC Version 1.0, may upgrade for \$225.

To order PC Version 2.0 or to obtain a license agreement for the database in magnetic-tape form, contact: Office of Standard Reference Data, A320 Physics Bldg., National Institute of Standards and Technology, Gaithersburg, MD 20899, telephone: 301/975-2208.

Calendar

May 3, 1989

SECOND ANNUAL DAMA SYMPOSIUM

Location: National Institute of
Standards and Technology
Gaithersburg, MD

The theme of this second symposium of the Data Administration Management Association, National Capital Region, is Data Administration: Standards and Techniques. Topics to be discussed will include the transition from business model to data model, quality data programs, bridging the gap between the strategic plan and systems development, data sharing and data integration issues in system development.

Contact: Judith Newton, A266 Technology Building, NIST, Gaithersburg, MD 20899, 301/975-3256.

May 4-5, 1989

9th CONFERENCE ON ROOFING TECHNOLOGY

Location: National Institute of
Standards and Technology
Gaithersburg, MD

The National Institute of Standards and Technology and the National Roofing Contractors Association have joined in sponsoring conferences on roofing technology on a biennial basis since 1969. This conference is the 9th Conference on Roofing Technology. The theme of the conference is Putting Roofing Technology to Work. Topics to be discussed include thermal analysis for membrane characterization, field testing and the effect of surface contamination on adhesive-bonded seams, compatibility of insulations and membranes, vapor retarders, thermal bridging, planned maintenance, and new developments in coatings.

Contact: Walt Rossiter, B348 Building Research Building, NIST, Gaithersburg, MD 20899, 301/975-6719.

June 7–9, 1989

**SECOND INTERNATIONAL
CONFERENCE ON HOT ISOSTATIC
PRESSING (HIP)—THEORY AND
APPLICATIONS**

Location: National Institute of
Standards and Technology
Gaithersburg, MD

During the last 15 years Hot Isostatic Pressing (HIP) has proved to be a versatile technique for the manufacture of advanced products, such as fully dense powder parts, and to increase the performance of components, e.g., defect healing of castings. The technique is evolving steadily. Significant advances are occurring in the modeling of the densification process, in the development of more versatile HIP units, and in the application of HIP technology to new types of materials. The goal of this conference is to promote a wider awareness of advances which have occurred since the previous conference in Lulea, Sweden in the theories and application of HIP, and to stimulate discussions of these advances and of the future directions for HIP technology. Sponsored by the National Institute of Standards and Technology.

Contact: Robert Schaefer, A153 Materials Building, NIST, Gaithersburg, MD 20899, 301/975-6162.

June 12-15, 1989

**INTERNATIONAL CONFERENCE ON
NARROW GAP SEMICONDUCTORS
AND RELATED MATERIALS**

Location: National Institute of
Standards and Technology
Gaithersburg, MD

Narrow gap semiconductors (NGS) have long been recognized for their special characteristics that create scientifically interesting effects and useful technological applications. The last NGS conference was held in Linz, Austria, in 1981. Since that time, new materials and new phenomena have been discovered (e.g., artificially structured materials grown by molecular beam epitaxy). The purpose of the conference is to bring together scientists and engineers interested in all aspects of narrow gap semiconductors and related materials.

The conference goals are to provide a forum in which topics of current interest and importance can be discussed and summarized and to act as an important stimulus for new progress in the field by providing new perspectives. Sponsored by the National Institute of Standards and Technology, the American Physical Society, the U.S. Air Force Office of Scientific Research, the Office of Naval Research, Texas Instruments, and the University of North Texas.

Contact: David G. Seiler, A305 Technology Building, NIST, Gaithersburg, MD 20899, 301/975-2081.

July 23–27, 1989

**SECOND INTERNATIONAL
CONFERENCE ON
CHEMICAL KINETICS**

Location: National Institute of
Standards and Technology
Gaithersburg, MD

The purpose of this conference is to bring together leading individuals from universities, research laboratories, and industrial organizations to review the progress and problems of current interest in the measurement, evaluation, and application of fundamental chemical kinetic data to the analysis of complex chemical processes. The conference will focus on those areas of science and technology in which modeling is being successfully used to explain and predict complex phenomena. Subject areas of interest include: atmospheric chemistry, acid deposition, combustion chemistry, chemistry of energetic materials, plasma processing, analytical chemistry, modeling studies of complex systems, experimental and theoretical approaches to providing fundamental chemical data, and the assembly and evaluation of data bases for large scale simulation of complex systems. The conference will be concerned with both gas and condensed phase chemistry. Sponsored by the National Institute of Standards and Technology, the U.S. Environmental Protection Agency, the National Aeronautics and Space Administration, the American Chemical Society, Petroleum Research Fund, the Gas Research Institute, the National Science Foundation, and the Ford Motor Company.

Contact: Rhoda Levin, A267 Chemistry Building, NIST, Gaithersburg, MD 20899, 301/975-2575.

September 19–21, 1989
**12th INTERNATIONAL
SYMPOSIUM ON POLYNUCLEAR
AROMATIC HYDROCARBONS**

Location: National Institute of
Standards and Technology
Gaithersburg, MD

The first 10 symposia on the chemistry and biochemistry of polynuclear hydrocarbons (PAH) were held on an annual basis and proved to be the major focal point for multidisciplinary research on this important class of chemical species. Since 1987, the meetings have been held biennially and continue to encourage open discussions between scientists representing government, academic institutions, industry, and research facilities investigating the chemical properties and biological effects of these compounds. The 1989 meeting will include presentations on parent hydrocarbon PAH as well as heteroatomic species, and PAH derivatives including amino, nitro, and halogen substituted compounds. Topics to be discussed include adducts, bioactivity, carcinogenesis, mutagenicity, cell transformation, detoxification, epidemiology, pollution modeling, occupational exposure, organic synthesis, and environmental studies. Sponsored by the National Institute of Standards and Technology, the National Institutes of Health, and Battelle Memorial Institute.

Contact: Willie E. May, A113 Chemistry Building, NIST, Gaithersburg, MD 20899, 301/975-3108.